Phosphorus sources for phosphatic Cambrian carbonates

Jessica R. Creveling[1,†], David T. Johnston[1,†], Simon W. Poulton[2], Benjamin Kotrc[1], Christian März[3], Daniel P. Schrag[1], and Andrew H. Knoll[1,4]

[1]*Department of Earth and Planetary Sciences, Harvard University, 20 Oxford Street, Cambridge, Massachusetts 02138, USA*
[2]*School of Earth and Environment, University of Leeds, Leeds, LS2 9JT, UK*
[3]*School of Civil Engineering and Geosciences, Newcastle University, Drummond Building, Newcastle upon Tyne, NE1 7RU, UK*
[4]*Department of Organismic and Evolutionary Biology, Harvard University, 26 Oxford Street, Cambridge, Massachusetts 02138, USA*

ABSTRACT

The fossilization of organic remains and shell material by calcium phosphate minerals provides an illuminating, but time-bounded, window into Ediacaran–Cambrian animal evolution. For reasons that remain unknown, phosphatic fossil preservation declined significantly through Cambrian Series 2. Here, we investigate the phosphorus (P) sources for phosphatic Cambrian carbonates, presenting sedimentological, petrographic, and geochemical data from the Cambrian Series 2–3 Thorntonia Limestone, Australia, some of the youngest Cambrian strata to display exceptional phosphatic preservation of small shelly fossils. We find that within Thorntonia sediments, phosphate was remobilized by organic decay and bacterial iron reduction, with subsequent reprecipitation largely as apatite within the interiors of small shelly fossils. We discuss the merits of bioclastic-derived, organic matter–bound, or iron-bound P as potential sources to these strata. Petrographic observations suggest that the dissolution of phosphatic skeletal material did not provide the P for fossil preservation. In contrast, high organic carbon contents imply significant organic fluxes of P to Thorntonia sediments. Sedimentology and iron-speciation data indicate that phosphorus enrichment occurred during times of expanded anoxic, ferruginous conditions in subsurface water masses, suggesting that phosphorus adsorption to iron minerals precipitating from the water column provided a second significant P source to Thorntonia sediments. Simple stoichiometric models suggest that, by themselves, neither organic carbon burial nor an iron shuttle can account for the observed phosphorus enrichment. Thus, we infer that both processes were necessary for the observed phosphorus enrichment and subsequent fossil preservation in the Thorntonia Limestone.

INTRODUCTION

Phosphorite and phosphatic carbonate define a spectrum of sedimentary lithologies enriched in the authigenic calcium phosphate mineral apatite (Kazakov, 1937; Baturin and Bezrukov, 1979; Riggs, 1986; Cook and Shergold, 1986; Cook et al., 1990; Föllmi, 1996; Trappe, 2001). The punctuated temporal distribution (Cook and McElhinny, 1979; Cook and Shergold, 1984, 1986) and evolving spatial distribution (Brasier and Callow, 2007) of phosphatic lithologies through Earth history suggest that unique and restrictive physical (Filippelli and Delaney, 1992) and/or chemical (e.g., Föllmi, 1996) conditions govern phosphate deposition in time and space.

There are many reasons to want to understand this distribution. Perhaps foremost is the practical concern for understanding how ore-grade sedimentary phosphorites form (e.g., Cook and Shergold, 1986). As with petroleum, phosphate ores are approaching peak production, while global demand continues to rise (Cordell et al., 2009; Filippelli, 2011). At the same time, biogeochemists increasingly invoke perturbations to the ancient phosphorus cycle to explain inferred fluctuations in biological productivity, organic carbon burial, and oxidant accumulation over geological time scales (Tyrrell, 1999; Bjerrum and Canfield, 2002; Saltzman, 2005; Holland, 2006; Konhauser et al., 2007; Algeo and Ingall, 2007; Planavsky et al., 2010; Swanson-Hysell et al., 2010). Finally, phosphatic deposits provide a direct window into evolutionary history through the exceptional preservation of fossils (Cook, 1992; Bengtson and Zhao, 1997; Xiao and Knoll, 2000; Butterfield, 2003; Porter, 2004a).

A global phosphogenic window coincides with major evolutionary innovation during the Ediacaran and Cambrian periods (Cook and Shergold, 1984, 1986; Cook, 1992). Much of our knowledge of early animal diversification derives from biomineralized and soft-bodied metazoans replaced and/or templated by phosphate minerals (Bengtson et al., 1990; Xiao and Knoll, 1999, 2000; Donoghue et al., 2006; Dornbos et al., 2006; Kouchinsky et al., 2012). Phosphatization taphonomy is tied to the biogeochemical cycle of phosphorus, and, for reasons that remain unknown, a major decline in the incidence of phosphatic lithologies and phosphatic fossil preservation occurred during Cambrian Series 2 (Cook and McElhinny, 1979; Porter, 2004b; Donoghue et al., 2006). To understand the loss of phosphatic lithologies, and the consequent closure of the Cambrian phosphatization taphonomic window, we must first understand how phosphorus entered the sediment column and how it was subsequently redistributed and concentrated around skeletal elements. In this paper, we ask specifically: What were the sources of phosphorus to phosphatic carbonates characterized by exceptional skeletal preservation?

Geochemistry provides one avenue to address this question. A common view holds that enhanced delivery of reactive phosphorus (i.e., phosphorus that may undergo biogeochemical transformations within the sediment column) to the seafloor was the primary variable governing the development of phosphatic lithologies (e.g., see Föllmi, 1996, and references therein; Papineau, 2010). In modern marine environments, the delivery of reactive phosphorus to the seafloor occurs predominantly in association with two phases (e.g., Delaney, 1998; Benitez-Nelson, 2000): phosphorus bound within organic matter (Redfield, 1958) and/or phosphorus adsorbed to or coprecipitated with particulate iron minerals (herein referred to as the "Fe-P shuttle"; Berner, 1973; Shaffer, 1986; Feely et al., 1991, 1998;

[†]E-mails: jcrevel@gps.caltech.edu; johnston@eps.harvard.edu

GSA Bulletin; January/February 2014; v. 126; no. 1/2; p. 145–163; doi:10.1130/B30819.1; 7 figures; Data Repository item 2013363.

Poulton and Canfield, 2006). To examine the extent to which these reactive phosphorus sources contributed to ancient phosphatic deposits, we report high-resolution phosphorus- and iron-speciation data, stable carbon isotope measurements, and trace-element concentrations for the phosphatic Thorntonia Limestone, Georgina Basin, Australia (Cambrian Series 2–3; Southgate, 1988; Southgate and Shergold, 1991), and, for comparison, the overlying nonphosphatic Arthur Creek Formation. We explore the possibility that bioclastic-bound, organic-bound, and iron-bound P provided the source for the Thorntonia phosphatic carbonates, and we develop simple mathematical models to assess the relative importance of organic- and iron-bound P. We find that while the high organic carbon content of the Thorntonia Limestone suggests that organic-bound P contributed significantly to authigenic apatite formation, C to P ratios indicate that organic-bound P was insufficient to account entirely for the observed phosphorus enrichment. Sedimentology and iron-speciation data indicate that these formations accumulated under anoxic, ferruginous subsurface water masses, allowing for the possibility that P adsorbed to iron minerals precipitating from the water column augmented organic-bound P delivery to the sediment column. Nonetheless, simple mathematical models indicate that, by itself, iron-bound phosphorus delivery is also incapable of accounting for the observed phosphorus enrichment. Thus, we infer that both organic-bound and iron-bound phosphorus sources were necessary for the development of the fossil-bearing phosphatic carbonates of the Thorntonia Limestone.

GEOLOGIC BACKGROUND

The Centralian Superbasin is a laterally extensive intracratonic basin that initiated during Neoproterozoic transcontinental rifting of Rodinia. Regional tectonic events subsequently dissected the superbasin into a mosaic of discrete, asymmetric, polyphase foreland basins (Fig. 1A; Walter et al., 1995; Lindsay, 2002; Dunster et al., 2007). Here, we focus on the phosphatic Cambrian strata of the southern Georgina Basin (Cook and Shergold, 1986; Southgate, 1988; Southgate and Shergold, 1991), which were deposited variably and diachronously across the basin (Cook and Shergold, 1986; Southgate, 1988; Howard, 1990; Southgate and Shergold, 1991; Dunster et al., 2007).

The Narpa Group encompasses Cambrian Series 2 and Series 3 stratigraphy of the southern Georgina Basin (Fig. 1B; Ambrose et al., 2001; Dunster et al., 2007). Deposition of its lowermost member, the phosphatic Thorntonia Limestone, reflects a major transgression and expansion of the Georgina Basin. For this reason, the basal contact of the Thorntonia Limestone can unconformably overlie the Shadow Group, conformably and gradationally overlie the Shadow Group, or overlie and rework crystalline basement (Fig. 1B). The rest of the Narpa Group records a basinwide, shallowing-upward succession that transitions from outer (lower Arthur Creek Formation), middle (upper Arthur Creek Formation), and inner ramp (Steamboat Sandstone) depositional environments into a flat-topped carbonate platform (Arrinthrunga Formation; Ambrose et al., 2001; Dunster et al., 2007).

Trilobite biostratigraphy assigns the Thorntonia Limestone to the Ordian and early Templetonian stages of Australian chronostratigraphy (Laurie, 2004a, 2004b; Dunster et al., 2007), correlative to Cambrian Series 2, Stage 4, and, possibly, lowermost Series 3, Stage 5 (Fig. 1B; Babcock and Peng, 2007; Peng and Babcock, 2011). Trilobite biozones within the Arthur Creek Formation are diagnostic for the Australian regional Ordian–Boomerangian stages (Laurie, 2004a, 2004b; Dunster et al., 2007), correlative to uppermost Stage 4 of Cambrian Series 2 through to the Guzhangian Stage of Cambrian Series 3 (Fig. 1B; Babcock and Peng, 2007; Peng and Babcock, 2011).

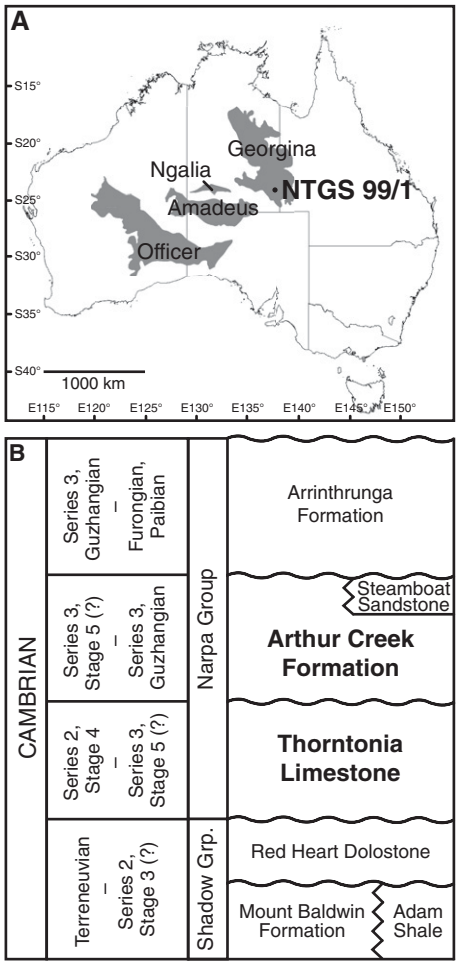

Figure 1. (A) Spatial extent of the constituent basins of the Neoproterozoic Centralian Superbasin. The black dot marks the drill locality for core NTGS 99/1 in the southern Georgina Basin. (B) Chronostratigraphy and lithostratigraphic nomenclature for the Northern Territory outcroppings of Cambrian strata within the southern Georgina Basin (modified from Dunster et al., 2007). The symbol "(?)" reflects uncertainties in correlating regional Australian trilobite zones with International Cambrian System designations.

METHODS

We examined the sedimentology and lithofacies associations of the Thorntonia Limestone and the Arthur Creek Formation within drill core Northern Territory Geological Survey (NTGS) 99/1 stored at the NTGS Core Facility, Alice Springs, Australia. With a water-cooled saw, we cut 534 quarter-core samples, 3-cm-long, perpendicular to bedding at ~10–25 cm resolution between 597.58 and 347.98 m core depth (mcd). Each sample was again divided (perpendicular to bedding) into two subsamples, one half designated as a hand-sample or thin-section billet, and the other half pulverized with a steel ring mill. Each hand-sample billet was microdrilled along individual laminations for carbonate carbon ($\delta^{13}C_{carb}$)

and carbonate oxygen ($\delta^{18}O_{carb}$) isotopic analysis. The evolved CO_2 was measured against an in-house reference gas on a VG Optima dual-inlet mass spectrometer attached to a VG Isocarb preparation system. We report isotopic values in Vienna Peedee belemnite (VPDB) per mil (‰) notation. Standard reproducibility was 1σ = <0.1‰ and 0.2‰ for $\delta^{13}C_{carb}$ and $\delta^{18}O_{carb}$, respectively.

Sample powders were divided for carbon, phosphorus, iron, and trace-element geochemical analyses aimed at diagnosing the sediment- and water-column geochemistry at the time of phosphatic carbonate deposition. To determine carbon mass fractions, we acidified 5–10 g of powdered sample with cold, 2.5 *M* hydrochloric acid. The resulting insoluble residue (i.e., the noncarbonate fraction, composed predominantly of siliciclastics and organic matter) was isolated by filtration, rinsed thoroughly with deionized water, and then dried and weighed. The total carbonate fraction was estimated as the weight percent difference between the bulk sample and the insoluble residue. To determine the weight percent of total organic carbon (TOC) and its isotopic composition ($\delta^{13}C_{org}$), aliquots of the insoluble residue were combusted within a Carlo Erba NA 1500 Analyzer attached to a Thermo Scientific Delta V Advantage isotope ratio mass spectrometer. Reproducibility of $\delta^{13}C_{org}$ for an acetanilide standard was 0.16‰ (1σ). Of the 100 samples processed, 29 were analyzed in duplicate and yielded an analytical reproducibility of 1σ = 0.07 wt% TOC. Finally, we estimated the weight percent of silicate phases (either clastic or authigenic) as the weight percent of the insoluble fraction minus the weight percent of the TOC fraction.

The speciation of phosphorus (P) was determined with a modified sequential extraction methodology for marine sediment (Ruttenberg, 1992). Here, 150–200 mg samples of rock powder were sequentially extracted with 10 mL each of (1) 0.3 *M* sodium-citrate, 1 *M* sodium bicarbonate, and 0.14 *M* sodium dithionite (pH = 7.5) for P bound to reducible/reactive ferric iron minerals (P_{Fe}), (2) 1 *M* sodium acetate (pH = 4.0) for carbonate fluorapatite, biogenic hydroxyapatite, and carbonate-bound P ($P_{auth+carb}$), (3) 1.2 *M* cold HCl for crystalline fluorapatite (P_{xl}), and (4) 1.2 *M* cold HCl after a 2 h ignition at 550 °C for organic P (P_{org}). To prevent P readsorption during the first two extraction steps, two 5 mL 1 *M* $MgCl_2$ washes were performed postextraction. Phosphorus in extracts and wash solutions (except P_{Fe}) was analyzed spectrophotometrically (Thermo Genesys 6) by the molybdate-blue method (Strickland and Parsons, 1972; Ruttenberg, 1992); P_{Fe} was measured by inductively coupled plasma–optical emission spectrometry (ICP-OES; Varian Vista-MPX). We note that Ruttenberg (1992) ascribes P-speciation phase 3, P_{xl}, to detrital fluorapatite of igneous and metamorphic origin. We abbreviate this phase as "xl" for "crystalline" so as to remove reference to a genetic mechanism (i.e., detrital) for an operationally defined phase based on a chemical extraction procedure. We hypothesize about the origin of this phase in greater detail in the discussion.

To verify the efficiency of the sequential extraction method, total P (P_T) values were determined independently (SGS Mineral Services Group, Toronto, ON, Canada) by inductively coupled plasma–atomic emissions spectrometry (ICP-AES) after a standard four-acid digestion ($HF\text{-}HClO_4\text{-}HCl\text{-}HNO_3$). These analyses also provided the additional major- and trace-metal concentrations reported herein. To account for variable dilution by siliciclastic influx, we report element concentrations normalized to aluminum (Al) in wt%/wt% and ppm/wt% units for major and trace elements, respectively.

To determine the speciation of iron within our samples, we applied a modified version of the sequential extraction method of Poulton and Canfield (2005). Here, 80–100 mg samples of rock powder were sequentially extracted with 10 mL each of (1) 1 *M* sodium acetate, adjusted to pH 4.5 with acetic acid to extract Fe associated with carbonate phases such as siderite and ankerite (Fe_{carb}); (2) 0.28 *M* sodium dithionite, adjusted to pH 4.8 with 0.2 *M* acetic acid and 0.25 *M* trisodium citrate, for iron oxides such as hematite and goethite (Fe_{ox}); and (3) 0.2 *M* ammonium oxalate and 0.17 *M* oxalic acid for magnetite (Fe_{mag}). The boiling chromium reduction distillation of Canfield et al. (1986) was used to quantify sulfur (S) within pyrite from the insoluble residues derived from carbonate dissolution. We used a pyrite stoichiometry (FeS_2) to relate the extracted S back to iron (Fe_{py}). Total Fe (Fe_T), which constitutes the sum of the diagenetically highly reactive phases ($Fe_{HR} = Fe_{carb} + Fe_{ox} + Fe_{mag} + Fe_{py}$), as well as unreactive Fe (Fe_U; predominately silicate-bound Fe), was determined via a boiling $HF\text{-}HNO_3\text{-}HClO_4$ extraction on an additional aliquot of sample powder. All iron concentrations were measured by atomic absorption spectrometry (AAS). Eight replicates of one sample, 572.64 mcd, yield a relative standard deviation (RSD) value of 2%, 13%, and 71% for Fe_{carb}, Fe_{ox}, and Fe_{mag}, respectively. The high RSDs of the latter two phases result from measured quantities close to the instrument detection limit; that is, the average wt% ± 1σ for the eight Fe-speciation replicates is 0.110 ± 0.002, 0.016 ± 0.002, and 0.001 ± 0.001 for Fe_{carb}, Fe_{ox}, and Fe_{mag}, respectively. At higher Fe concentrations for each fraction, the RSD is <5% for each stage, and this is also the case for Fe_{py} and Fe_T (Poulton and Canfield, 2005).

RESULTS

Lithofacies Descriptions and Paleoenvironmental Interpretations for the Thorntonia Limestone and Arthur Creek Formation from Drill Core NTGS 99/1

Markings on drill core NTGS 99/1 assign 598.4–580.1 mcd, 580.1–558.7 mcd, and 558.7–554.7 mcd to the informal lower, middle, and upper members, respectively, of the Thorntonia Limestone (previously Hay River Formation), and 554.7–103.2 mcd to the Arthur Creek Formation (previously Marqua Formation; Ambrose et al., 2001; Dunster et al., 2007). In this study, we characterized the sedimentology and geochemistry of the entire Thorntonia Limestone and the lowermost ~200 m of the lower Arthur Creek Formation.

Thorntonia Limestone

The Shadow Group is absent from NTGS 99/1. Here, the Thorntonia Limestone directly overlies Paleoproterozoic granite basement. The basal meters of the lower Thorntonia member include lithic fragments and sand grains within dolomudstone, with minor cubic pyrite crystals (Fig. 2A). More generally, the lower Thorntonia consists of dolomudstone and peloidal dolowackestone, with pervasive structural dissolution textures creating a stylolaminated to stylobedded fabric (Fig. 2B). Southgate and Shergold (1991) designated the basal, arkosic, terrigenous unit as a lowstand system tract, and the overlying stylolitic carbonate as a condensed transgressive or highstand system tract.

Below 580.1 mcd (the lower Thorntonia Limestone) and from 580.1 to 575.92 mcd (the lowermost middle Thorntonia Limestone), the bulk lithology is dolostone. Stratigraphically above this horizon, up to the middle–upper Thorntonia Limestone contact at 558.7 mcd, the bulk lithology is limestone. Nevertheless, petrographic observation of the bulk limestone lithofacies above 575.92 mcd reveals rare euhedral dolomite rhombs within an otherwise calcimudstone or calciwackestone matrix.

The middle Thorntonia contains four interbedded and interlaminated lithofacies that occur within generally coarsening-upward meter- to submeter-scale packages (Fig. 2C). These lithofacies include: (1) black to medium-gray carbonate mudstone; (2) dark- to medium-gray peloidal, bioclastic, and, occasionally, intraclastic wackestone; (3) medium- to light-gray peloidal and bioclastic packstone; and (4) medium- to light-gray

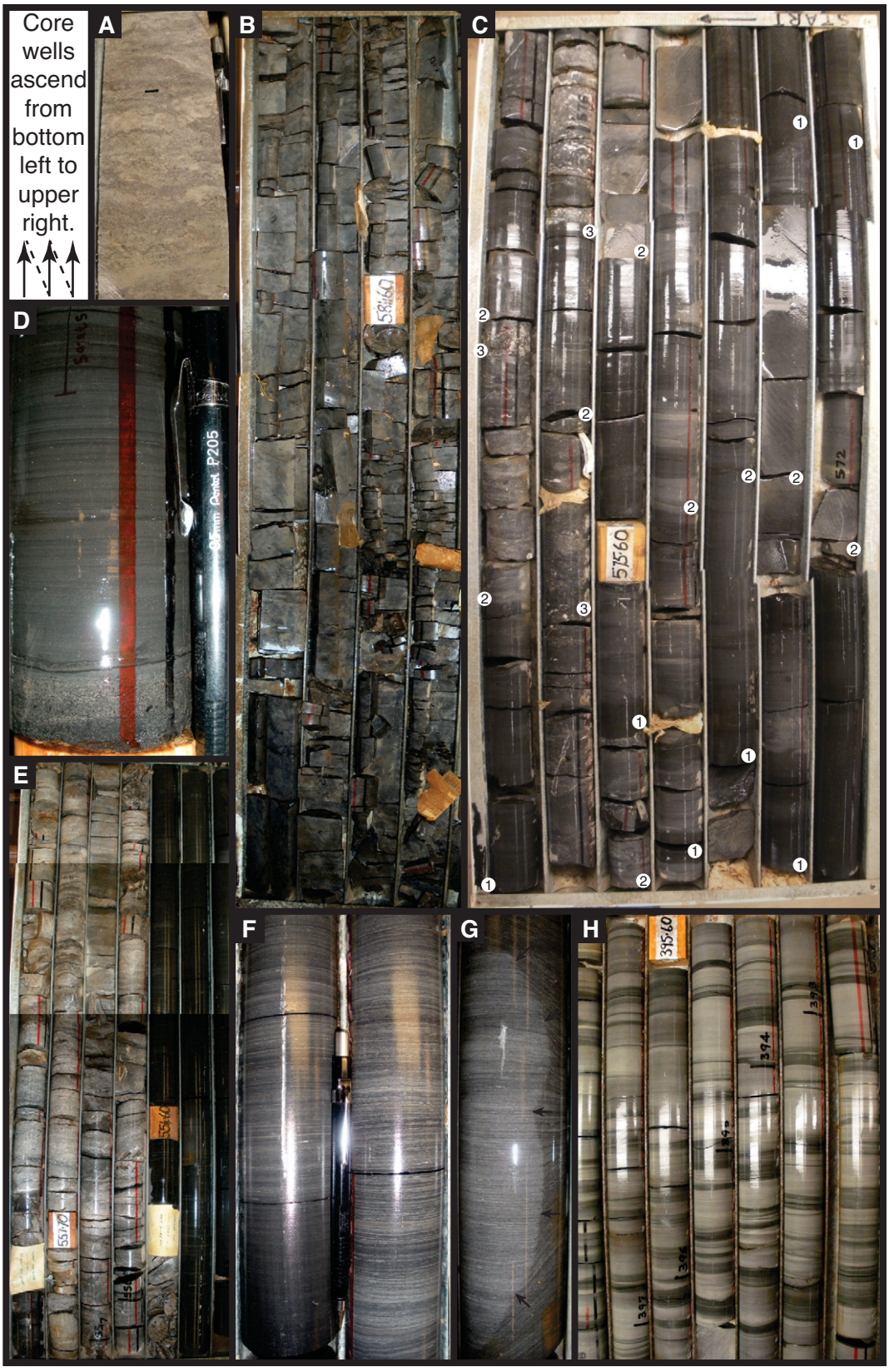

Figure 2. Lithofacies of the Thorntonia Limestone and Arthur Creek Formation in NTGS 99/1. (A) Sandy dolostone of the lower Thorntonia Limestone, just above the contact with the underlying Paleoproterozoic granite basement (~595.8–595.6 mcd). (B) General character of the mottled-to-stylonodular, dolomitic lower Thorntonia Limestone (584–580.5 mcd). (C) Characteristic meter- to submeter-scale lithologic alternations and color variation within limestone of the middle Thorntonia Limestone (577.7–571.4 mcd). (1) Denotes black and dark gray calcimudstone; (2) denotes lighter-gray calcimudstone, wackestone, and packstone; and (3) denotes limestone grainstone. Note the general up-package coarsening and lightening, often without cyclic or predictable variation. (D) Bioclastic grainstone to mudstone transition from 570.15 to 570.05 mcd (middle Thorntonia Limestone; all limestone). (E) Appearance of the vuggy, bioclastic dolomitic grainstone of the upper Thorntonia Limestone (left) and the overlying basal "hot shale" of the lower Arthur Creek Formation (right). Contact at 554.7 mcd. (F) The laminated siliciclastic shale/siltstone and calcimudstone facies of the lower Arthur Creek Formation. (G) Light-gray early diagenetic nodule (calcimudstone) displacing dark-gray laminations within the lower Arthur Creek Formation at 532.8–532.65 mcd (arrows mark the exterior of the nodule). (H) General appearance of the interbedded siliciclastic mudstone/siltstone and calcimudstone (neomorphosed to microspar) facies of the lower Arthur Creek Formation above ~430 mcd.

bioclastic grainstone. Carbonate mudstone or wackestone lithofacies define the base of each package and interlaminate or alternate gradationally on a centimeter to decimeter scale. These carbonate mud–dominated lithologies typically grade upward into, and contact sharply with, laminae and beds of packstone. When present, thin beds of bioclastic grainstone overlie packstone beds. These grainstone beds display basal erosional contacts with millimeter- to half-centimeter-scale topography, and an upper contact that is either sharp or erosional and overlain by beds of black to medium-gray carbonate mudstone. In other cases, the upper contact is diffuse and conformable with beds of medium-gray packstone or wackestone (Fig. 2D). There is a broad up-core trend: Packages initiate with progressively coarser lithologies and terminate with progressively thicker grainstone beds. The nature of deposition of the Thorntonia Limestone within NTGS 99/1 is consistent with the phosphatic lithofacies model from the northeast Georgina Basin (Cycle mP of Southgate, 1988). Southgate and Shergold (1991) assigned these shallowing-upward cycles to the transgressive system tract.

We interpret the lithologic association of the middle Thorntonia Limestone to reflect deposition within a subtidal to intertidal depositional environment. Mudstone, wackestone, and packstone beds accumulated from suspension sedimentation in calm settings that lacked significant tidal, wave, or storm activity. The coarser grain size and subtle current-generated stratification observed in grainstone beds reflect a higher-energy depositional environment. Grainstone beds reveal no internal grading, but they do show evidence for amalgamation and winnowing of carbonate mud by currents or waves. Deposition under the influence of waves is also manifest in rosettes of brachiopod and trilobite shell fragments along basal scour surfaces of bioclastic grainstone beds (Fig. 2D). Dunster et al. (2007) interpreted the black, carbonaceous carbonates of the Thorntonia Limestone to represent deposition under dysoxic to anoxic conditions.

In NTGS 99/1, the upper Thorntonia Limestone encompasses a 4-m-thick vuggy, fossiliferous dolopackstone with laminae, beds, and pockets of bioclastic dolograinstone (Fig. 2E). When present, dolospar crystals form a mosaic around bioclasts (primarily of lingulate brachiopods). In addition to representing a prominent matrix constituent, bioclasts occur as cumulate along dissolution seams.

Petrography of apatite distribution. Apatite displays three predominant modes within the middle and upper Thorntonia Limestone. First, within bioclast-rich carbonate lithologies, apatite occurs primarily as the internal molds (steinkerns) of conical small shelly fossils or, more commonly in the upper Thorntonia Limestone, as lingulate brachiopod skeletal debris (Fig. 3A). Apatite also occludes gaps between, and templates the exterior of, silica-replaced skeletons (Fig. 3A). Second, in rare instances, apatite occurs as cement within bioclastic grainstone lithologies (Fig. 3B), Third, within mud-supported, suspension-deposited carbonate, apatite occurs as subangular to subrounded coarse-silt– to medium-sand–size grains, and as silt- to fine-sand–size, tabular or undulose grains within well-sorted, thin beds (Fig. 3C). Due to the textural maturity and fine grain size of these lithologies, we cannot say conclusively whether these grains were eroded, transported, and winnowed from a site of apatite authigenesis (i.e., allochthonous apatite grains) or whether they arrived with a detrital siliciclastic influx. We favor the interpretation that these grains represent reworked authigenic grains (i.e., intraclasts of authigenic cement and steinkern bio-

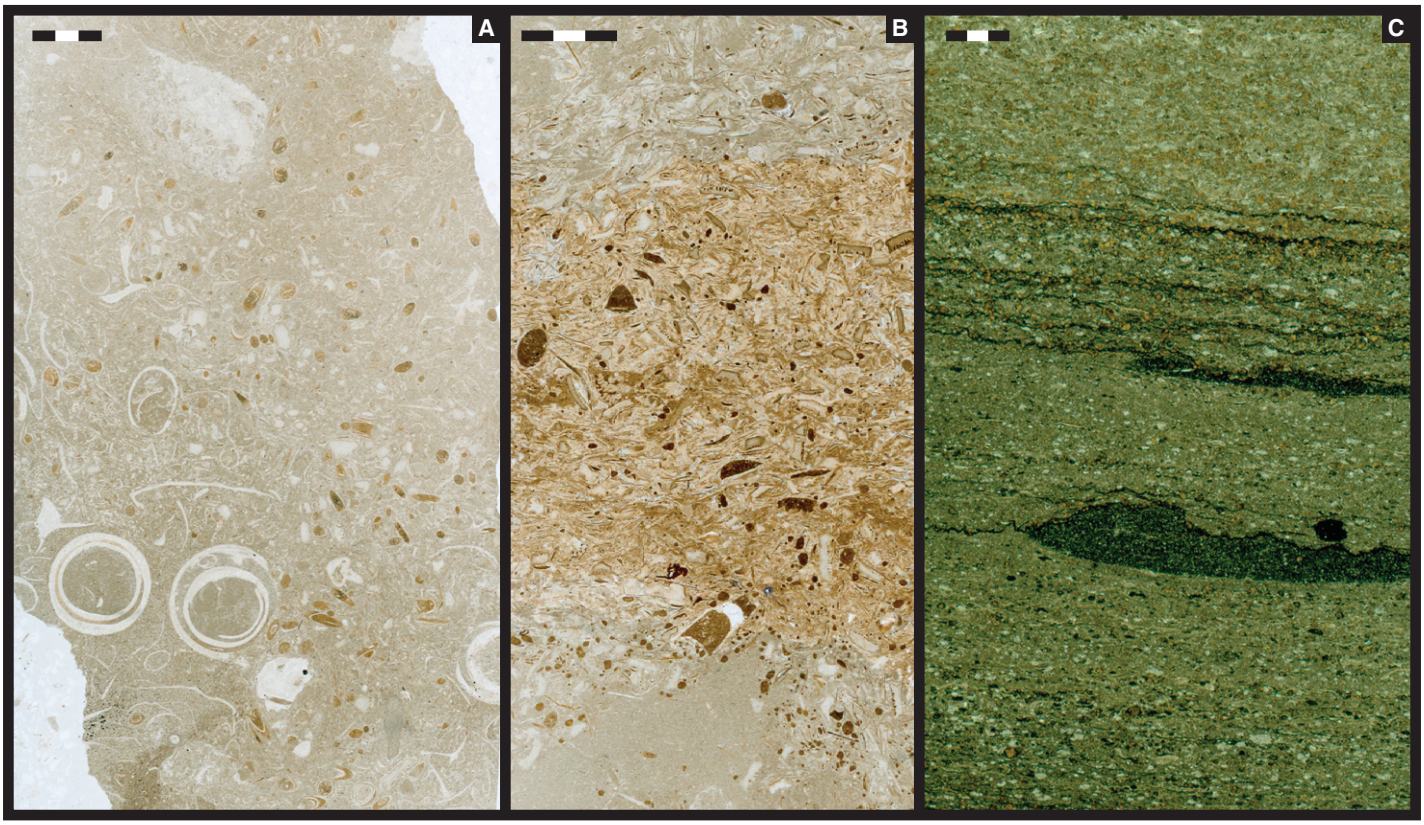

Figure 3. Photomicrographs under plane-polarized light of authigenic apatite distribution within the middle Thorntonia Limestone. (A) A limestone packstone with apatite replacement specifically targeting the interior of conical small shelly fossil elements at 570.35 mcd. (B) Wholesale cement and grain phosphatization of a limestone at 575.17 mcd. (C) Dispersed, allochthonous grains of authigenic apatite within a limestone at 560.69 mcd (see text for discussion of origin). The scale bar in each frame is 3 mm.

clasts) because we observe no comparable-size detrital siliciclastic grains. Later herein, we discuss the origin of these grains in light of geochemical data (see section titled, "Source(s) of Phosphorus to the Thorntonia Limestone and Arthur Creek Formation").

Arthur Creek Formation

Within NTGS 99/1, the basal 10 m of the lower Arthur Creek encompasses a petroleum-generating, massive black shale (Fig. 2E), or "hot shale" (e.g., Dunster et al., 2007), succeeded by planar, undulose, and corrugated interlaminae of black to dark-gray organic matter– and clay-rich shale and siltstone with medium- to light-gray calcimudstone and dolomudstone. This shale also contains rare interbeds of very fine-grained bioclastic packstone and grainstone (Fig. 2F). Clay- and iron-oxide–rich laminae include subrounded to angular, very well-sorted, monocrystalline quartz and authigenic pyrite crystals, the latter of which often occlude pore space. Horizontal alignment of clay minerals indicates that compaction enhanced the physical expression of lamination. Commonly below ~490 mcd, and only rarely above, decimeter-scale light-gray limestone nodules displace surrounding laminations and retain faint remnants of lamination, indicating nodular development during compaction, but before lithification (Fig. 2G). We interpret individual laminae to reflect the gravitational settling of fine particles suspended by dilute turbidity currents that wafted sediment toward the basin interior, consistent with an outer-ramp depositional environment (Dunster et al., 2007). The fetid, carbonaceous black shale and black, carbonaceous, laminated dolostone suggest deposition under dysoxic to anoxic conditions (Dunster et al., 2007).

In the upper meters of the measured lower Arthur Creek, a second lithofacies interbeds with the laminated facies (Fig. 2H). This facies includes interbeds of light-gray calcimudstone and siliciclastic siltstone. Rare truncation of undulatory laminae indicates intermittent deposition under the influence of currents. This facies is a harbinger of the more proximal, oxygenated ramp environment of the overlying upper Arthur Creek Formation (Dunster et al., 2007), which was not measured in this study. Southgate and Shergold (1991) assigned the lower Arthur Creek to a transgressive system tract.

Geochemistry of the Thorntonia Limestone and Arthur Creek Formation

A generalized stratigraphic column of the Thorntonia Limestone and the lower Arthur Creek Formation from drill core NTGS 99/1 is shown in Figure 4A alongside chemostratigraphic variation in $\delta^{13}C_{carb}$ (Fig. 4B), $\delta^{18}O_{carb}$ (Fig. 4C), and $\delta^{13}C_{org}$ (Fig. 4D). Cross-plots of $\delta^{13}C_{carb}$ and $\delta^{18}O_{carb}$ display no statistically significant covariation (Fig. 4E), thereby suggesting that $\delta^{13}C_{carb}$ values, at least, represent the primary seawater isotopic composition. The $\delta^{13}C_{carb}$ curve generated for NTGS 99/1 displays two positive peaks, the first in the middle Thorntonia (563.92 mcd) and the second in the Arthur Creek (506.51 mcd). Consistent with trilobite biostratigraphy (Laurie, 2004a, 2004b), we correlate the middle Thorntonia excursion to the Ordian–early Templetonian isotopic event and the Arthur Creek excursion to the late Templetonian–Floran event (Fig. 4B; Lindsay et al., 2005). This assignment corroborates regional isotopic variation in the southern Georgina, Amadeus, and Daly Basins (Lindsay et al., 2005) and, further afield, in the Argentine Precordillera (Gomez et al., 2007), the Great Basin, United States (Saltzman, 2005), South China (Zhu et al., 2004; Guo et al., 2010), and northwest China (Wang et al., 2011).

Small-magnitude discontinuities in $\delta^{13}C_{carb}$ chemostratigraphy occur across the informal member boundaries of the Thorntonia Limestone (Fig. 4B). These discontinuities likely represent erosive events or hiatuses in deposition. In support of the former interpretation, an increase in Zr/Al occurs across the middle-upper Thorntonia contact (Fig. DR1[1]). Elevated Zr/Al ratios define erosional surfaces where high-energy currents winnowed fine-grained, low-density siliciclastics (characterized by Al) and concentrated high-density minerals (characterized by Zr; Vine and Tourtelot, 1970). Unlike carbon isotopes, secondary fluid migration does not affect the Zr/Al ratio. Thus, this proxy confirms sediment winnowing during deposition of the upper Thorntonia Limestone. Regionally, the Thorntonia Limestone–Arthur Creek Formation contact represents a sequence boundary, with karstification developed along this surface in the western margin of the basin (Dunster et al., 2007). While the formation boundary within NTGS 99/1 represents a sharp lithologic break, $\delta^{13}C_{carb}$ values display general continuity across this boundary (Fig. 4B), suggesting either relative temporal continuity or fortuitous resumption of deposition with similar carbon isotopic composition. Isopach maps of the Arthur Creek Formation show that the formation thickens to the east-southeast, where the NTGS 99/1 drill core intercepted the maximum depocenter of the preserved basin margin (Dunster et al., 2007). Thus, under the former scenario, the Thorntonia Limestone–Arthur Creek Formation boundary within NTGS 99/1 could represent a correlative conformity of the regional sequence boundary, with limited time missing across this lithologic contact.

Within NTGS 99/1, $\delta^{13}C_{org}$ displays covariation with $\delta^{13}C_{carb}$ within the lower Thorntonia Limestone and no covariation with $\delta^{13}C_{carb}$ within either the middle-upper Thorntonia Limestone or the Arthur Creek Formation (Figs. 4D and 4F; lower Thorntonia: $R^2 = 0.75$; middle-upper Thorntonia: $R^2 = 0.04$; Arthur Creek: $R^2 = 0.2$). TOC varies from 0.1 to 2.9 wt% in the Thorntonia Limestone, displaying a generally increasing trend in the lower Thorntonia and high variance in the middle Thorntonia. TOC ranges from 0.1 to 2.5 wt% in the lower Arthur Creek Formation, with higher values at the base of the formation, decreasing toward a mean of 0.1 wt% TOC in the upper 100 m of the measured core interval (Fig. 4D). Despite the lack of covariance between $\delta^{13}C_{carb}$ and $\delta^{13}C_{org}$ in strata of the middle-upper Thorntonia and the Arthur Creek Formation, one trend emerges: High (>1.0 wt%), medium (0.2 < wt% < 1.0), and low (<0.2 wt%) TOC values correlate with light, intermediate, and heavy $\delta^{13}C_{org}$ values (Fig. 4D). That is, the lightest $\delta^{13}C_{org}$ values occur in the most organic- and phosphorus-rich lithofacies, the middle Thorntonia Limestone (cf. Bartley et al., 1998; Guo et al., 2013). The latter two TOC bins generally correspond to samples from the Arthur Creek below and above ~430 mcd, respectively, which is the transition between the laminated facies and the interbedded carbonate mudstone–siliciclastic shale and siltstone facies.

Total phosphorus (P_T) within the Thorntonia Limestone ranges up to 3.9 wt% (Fig. 5A). P_T increases systematically within the lower Thorntonia and the lowermost middle Thorntonia Limestone, followed by an additional increase around 575 mcd. We note that the transition from dolostone (stratigraphically below 575.92 mcd) to limestone (stratigraphically above 575.92 mcd) within drill core NTGS 99/1 occurs just below this jump in P content (Figs. 5A and 5B). The overlying meters of the middle and upper Thorntonia Limestone display high variance in P_T. In contrast, the maximum value of P_T within the Arthur Creek Formation is 0.4 wt%, but values are typically much lower, with a median of 0.03 wt% and first and third quartile values of 0.02 and 0.04 wt%, respectively (Fig. 5A).

We tested the fidelity of the P sequential extraction method by comparing the sum of the operationally defined pools ($P_T = P_{xl} + P_{auth+carb} + P_{org} + P_{Fe}$) to the total phosphorus content determined by ICP-AES analysis. The consistency between these two measurement techniques (slope of linear regression = 1.1, $R^2 = 0.88$; Fig. 5E) increases our confidence in the values

[1]GSA Data Repository item 2013363, two figures and an accompanying discussion of additional bulk and aluminum-normalized trace element geochemical data, is available at http://www.geosociety.org/pubs/ft2013.htm or by request to editing@geosociety.org.

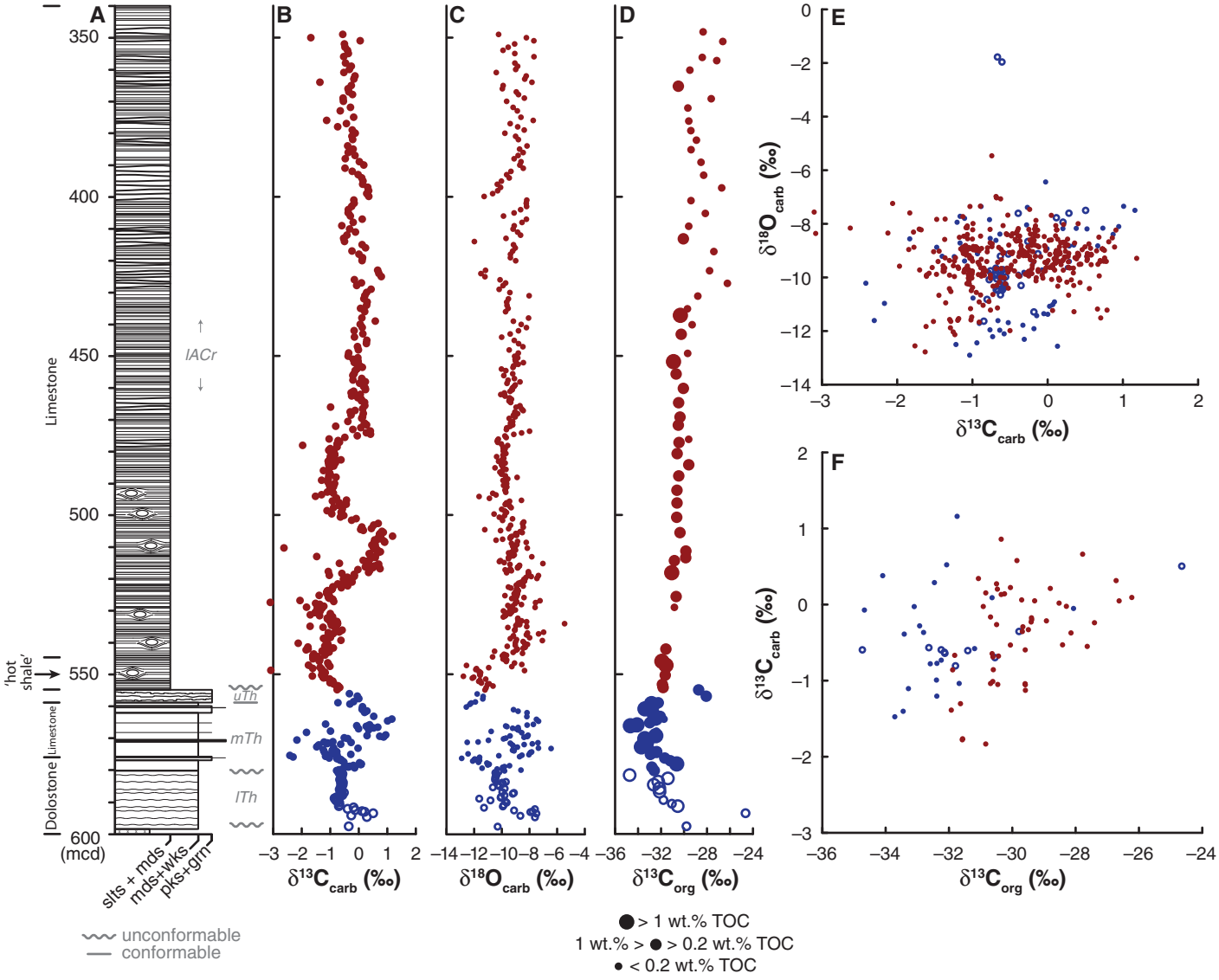

Figure 4. Lithology and stable isotope chemostratigraphy of the Thorntonia Limestone and lower Arthur Creek Formation within drill core NTGS 99/1. For all panels, data for the lower and middle-upper Thorntonia Limestone are plotted in open and solid blue circles, respectively, while data for the Arthur Creek Formation are plotted in solid red circles. (A) Generalized stratigraphic column depicting the lithology of the lower, middle, and upper Thorntonia Limestone (lTh, mTh, and uTh, respectively) and the lower Arthur Creek Formation (lACr). Lithologic abbreviations: Siliciclastics: slts—siltstone; Carbonates: mds—mudstone; wks—wackestone; pks—packstone; grn—grainstone. Vertical axis reflects meters core depth from the surface. (B) Carbonate carbon isotopic composition (relative to Vienna Peedee belemnite [VPDB]). (C) Carbonate oxygen isotopic composition (relative to VPDB). (D) Total organic carbon isotopic composition (symbol size scaled to wt% total organic carbon [TOC]). (E) Cross-plot of carbonate carbon and carbonate oxygen isotopic composition. (F) Cross-plot of organic carbon and carbonate carbon isotopic composition.

of the constituent sequential extraction phases. In both the Thorntonia Limestone and the Arthur Creek Formation, the operationally defined P_{xl} and $P_{auth+carb}$ phases dominate P_T, while P_{org} and P_{Fe} contribute a negligible fraction (Fig. 5B). The median (first, third quartile) percent contributions to P_T are: P_{xl} = 91.5% (77.5, 94.4), $P_{auth+carb}$ = 7.5% (3.7, 19.5), and P_{org} = 0.4% (0.2, 1.5). P_{Fe} was measured only on a subset of samples, but this phase contributes minimally to P_T (a median of 0.1% with first and third quartiles of 0.0% and 0.4%, respectively).

Total iron (Fe_T) varies from 0.06 to 1.49 wt% in the Thorntonia Limestone and from 0.32 to 2.71 wt% in the Arthur Creek Formation (Fig. 5C). In general, Fe_T is lowest where P_T is highest. Based on the slope of linear regression, 88% of Fe_T resides in Fe_{HR} phases within the Thorntonia Limestone (R^2 = 0.92; Fig. 6A). In contrast, within the Arthur Creek Formation, ~48% of Fe_T resides in Fe_{HR} (R^2 = 0.57; Fig. 6A), consistent with the higher siliciclastic fraction for these lithologies. The lower coefficient of determination for the Arthur Creek Formation reflects a decrease in Fe_{HR}/Fe_T from 0.66 at the base of the formation to ~0.3 near the top of the measured core interval. Reduced iron phases, Fe_{py} and Fe_{carb}, dominate Fe_{HR} in both formations, while oxidized and partially oxidized iron phases, Fe_{ox} and Fe_{mag}, contribute a minimal fraction (Fig. 5C). Based on

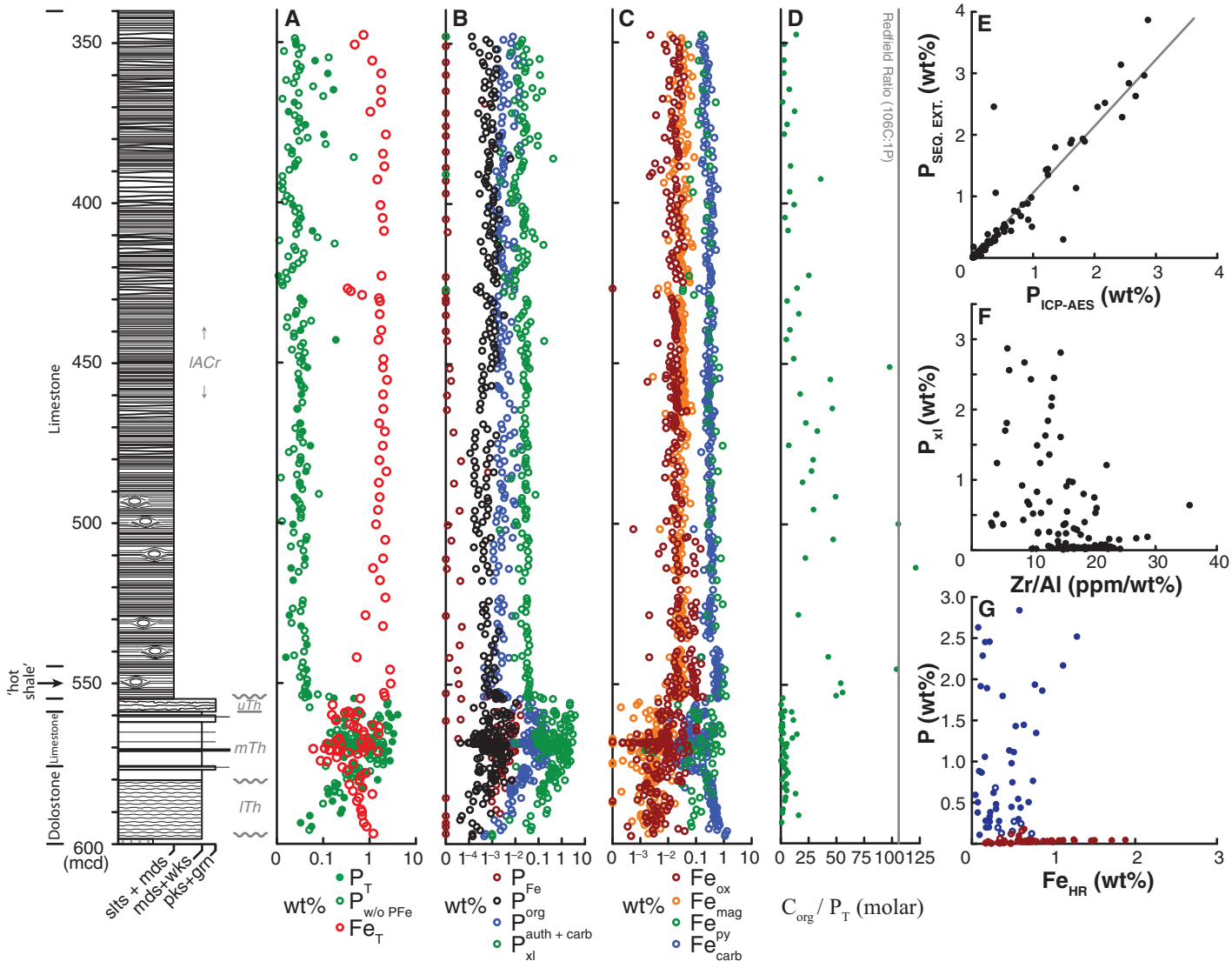

Figure 5. Phosphorus and iron-speciation geochemistry, molar C:P ratios, and correlations between P and other geochemical metrics within the Thorntonia Limestone and Arthur Creek Formation. Stratigraphic column at left same as in Figure 4 (see Fig. 4 for abbreviations). (A) The weight percent of total phosphorus (filled green circles) and subtotal phosphorus (open green circles) for those samples for which P_{Fe} concentrations were not determined from P-speciation geochemistry. Weight percent total Fe (open red circles) from iron-speciation geochemistry. Note the logarithmic scale to emphasize, in particular, the P content of the middle and upper Thorntonia Limestone. (B) The weight percents of operationally defined phosphorus phases as determined by phosphorus-speciation geochemistry. Note the logarithmic scale. See text for discussion of the operationally defined P phases. (C) The weight percents of iron phases as determined by iron-speciation geochemistry. Note the logarithmic scale. (D) The molar ratio of organic carbon to total phosphorus. Gray line intersects the axis at C:P = 106:1, the canonical Redfield ratio. (E) Correlation between the weight percent phosphorus within individual samples as determined from inductively coupled plasma–atomic emission spectrometry (ICP-AES) versus that determined by the sequential extraction method (Seq. Ext.; see Methods section). Slope of linear regression = 1.1; R^2 = 0.88. (F) Correlation between the zirconium to aluminum ratio (Zr/Al, ppm/%) and the operationally defined P_{xl} phase (see text for discussion) determined from phosphorus-speciation geochemistry. (G) Cross-plot of the weight percent of highly reactive iron species (Fe_{HR}; oxides, magnetite, pyrite, and iron carbonates) determined from iron-speciation geochemistry versus the weight percent of total phosphorus determined from phosphorous-speciation geochemistry. Data for the lower and middle-upper Thorntonia Limestone are plotted in open and solid blue circles, respectively, while data for the Arthur Creek Formation are plotted in solid red circles.

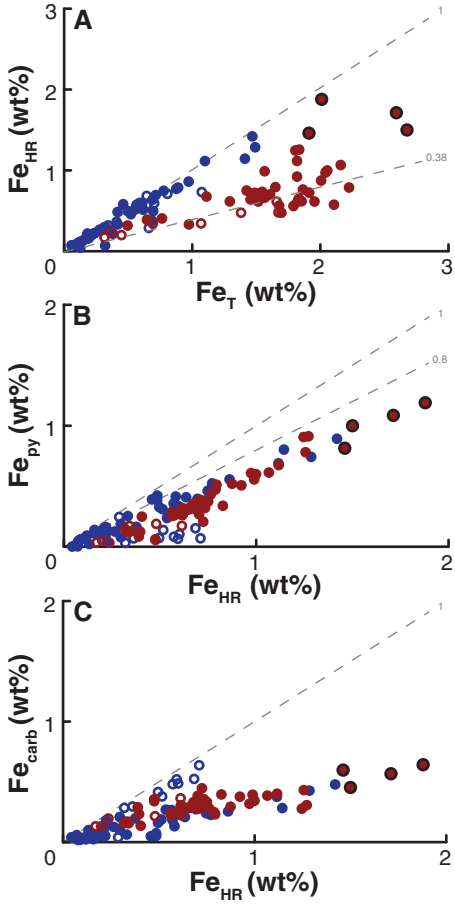

Figure 6. Iron-speciation geochemistry. For all panels, data for the lower and middle-upper Thorntonia Limestone are plotted in open and solid blue circles, respectively, while data for the laminated facies and interbedded siliciclastic/carbonate mudstone facies of the Arthur Creek Formation are plotted in solid and open red circles, respectively. Data from the Arthur Creek "hot shale" appear as solid red circles with a black outline. (A) A cross-plot of the weight percent total iron (Fe_T) versus the weight percent iron within highly reactive phases (Fe_{HR}; oxides, magnetite, pyrite, and iron carbonates). We plot slopes of 1 and 0.38 as a reference for comparing these carbonate data to previously published iron-speciation data, but we do not advocate interpreting carbonate data (blue circles) within the canonical siliciclastic framework. Slopes of regressions (not plotted) reflect the percentage of the total iron residing in highly reactive phases (lower Thorntonia = 57%, R^2 = 0.53; middle-upper Thorntonia = 89%, R^2 = 0.95; laminated facies of the Arthur Creek = 53%, R^2 = 0.44; interbedded siliciclastic shale/siltstone and carbonate mudstone facies of the Arthur Creek = 26%, R^2 = 0.90). (B) A cross-plot of the weight percent highly reactive iron (Fe_{HR}) versus the weight percent iron within pyrite (Fe_{py}). We plot slopes of 1 and 0.8 for reference (see A). Slopes of regressions (not plotted) reflect the percentage of the highly reactive iron residing within pyrite (lower Thorntonia = 17%, R^2 = 0.07; middle-upper Thorntonia = 64%, R^2 = 0.95; laminated facies of the Arthur Creek = 75%, R^2 = 0.95; interbedded siliciclastic shale/siltstone and carbonate mudstone facies of the Arthur Creek = 30%, R^2 = 0.50). We note that the linear regression for the "hot shale" ($Fe_{py} = 0.8 \times [Fe_{HR}] - 0.2$) is the same for the lower Arthur Creek laminated facies exclusive of the hot shale data. (C) A cross-plot of the weight percent highly reactive iron (Fe_{HR}) versus iron carbonate (Fe_{carb}). Slopes of regressions (not plotted) reflect the percentage of the highly reactive iron residing within iron carbonate (lower Thorntonia = 82%, R^2 = 0.62; middle-upper Thorntonia = 31%, R^2 = 0.82; laminated facies of the Arthur Creek = 25%, R^2 = 0.68; interbedded siliciclastic shale/siltstone and carbonate mudstone facies of the Arthur Creek = 52%, R^2 = 0.73). We note that the linear regression for the hot shale ($Fe_{carb} = 0.25 \times [Fe_{HR}] + 0.15$) is similar for the lower Arthur Creek laminated facies exclusive of the hot shale data ($Fe_{carb} = 0.20 \times [Fe_{HR}] + 0.15$).

the slope of the linear regression, 82% of Fe_{HR} resides as Fe_{carb} within the lower Thorntonia Limestone (R^2 = 0.62; Fig. 6C), while Fe_{py} accounts for only a minor contribution that has no statistically significant correlation with Fe_{HR} (Fig. 6B). As such, the gradual decrease in Fe_{HR} within the lower Thorntonia Limestone reflects a systematic decrease in Fe_{carb} from very high values of 1.3 wt%, to ~0.3 wt%. In the middle and upper Thorntonia, 64% of Fe_{HR} resides as Fe_{py} (R^2 = 0.95; Fig. 6B), and 31% resides as Fe_{carb} (R^2 = 0.82; Fig. 6C). For the lower Arthur Creek Formation, ~73% and 26% of Fe_{HR} reside in Fe_{py} (R^2 = 0.94; Fig. 6B) and Fe_{carb} (R^2 = 0.72; Fig. 6C), respectively.

When we parse the Fe-speciation data of the middle Thorntonia Limestone samples by lithology, we see a similar partitioning of Fe phases as when we group all samples within members (as already presented). Within the dolostone of the middle Thorntonia Limestone (580.1–575.92 mcd), 98% of Fe_T resides in Fe_{HR} (R^2 = 0.99); in contrast, within the limestone of the middle Thorntonia section (575.92–558.7 mcd), 89% of Fe_T resides in Fe_{HR} (R^2 = 0.95). Likewise, within middle Thorntonia dolostone, 67% (R^2 = 0.94) and 27% (R^2 = 0.69) of Fe_{HR} reside in Fe_{py} and Fe_{carb}, respectively; within the middle Thorntonia limestone, 68% (R^2 = 0.96) and 30% (R^2 = 0.86) of Fe_{HR} reside in Fe_{py} and Fe_{carb}, respectively.

Within NTGS 99/1, the median (first, third quartile) percent acid-insoluble fraction (i.e., silicates) within the Thorntonia Limestone is 8.3% (5.3, 17.0), as compared to 44.0% (32.8, 54.3) for the Arthur Creek Formation (Fig. DR1 [see footnote 1]). TOC/Al ratios are higher and more variable in the Thorntonia Limestone than for the Arthur Creek Formation (Fig. DR1 [see footnote 1]). Fe/Al ratios and Mn/Al ratios decline throughout the lower Thorntonia Limestone (save for a couple of high values in the upper Thorntonia Limestone; Fig. DR1 [see footnote 1]). The detrital-associated trace-element ratio Zr/Al is low and variable within the Thorntonia Limestone compared to the Arthur Creek Formation and displays an abrupt increase across the middle-upper Thorntonia boundary. (See supplementary information for a discussion of aluminum-normalized concentrations of redox-sensitive and bioessential trace metals; Fig. DR2 [see footnote 1].)

DISCUSSION

How do these geochemical data inform our understanding of the source of phosphorus to phosphatic Thorntonia carbonates and, more broadly, the loss of phosphatic lithologies and consequent closure of the phosphatization taphonomic mode during Cambrian Series 2? To address these questions, we combine petrographic observations with P-speciation data to quantify authigenic apatite within the Thorntonia Limestone. In turn, we explore the possibility that P bound within bioclasts, organic matter, or iron minerals provided the observed P within these lithologies. Finally, we present a mathematical framework in which to deconvolve the relative contribution of the two most likely sources—P bound with organic matter or iron minerals—to authigenic apatite nucleation.

Source(s) of Phosphorus to the Thorntonia Limestone and Arthur Creek Formation

How much of the apatite within the Thorntonia Limestone and Arthur Creek Formation must we account for with P delivery shuttles? Phosphorus speciation provides a (semi)quantitative measure of the partitioning of

phosphorus within a sedimentary succession. The majority of P extracted from NTGS 99/1 is operationally classified as fluorapatite of detrital igneous and/or metamorphic origin (P_{xl}; Ruttenberg, 1992) and constitutes a median (first, third quartile) of 91.5% (77.5, 94.4) of P_T. However, we have three reasons to question this genetic interpretation. First, as described earlier, petrographic observations reveal that apatite within the Thorntonia Limestone occurs predominantly as the internal molds of small shelly fossils (Fig. 3A) or, occasionally, as cement within bioclastic grainstone (Fig. 3B), both indications of an authigenic origin. Given the thermal history of the Georgina Basin, which reached temperatures necessary to develop Type II kerogen (Dunster et al., 2007), burial diagenesis should have increased the crystallinity of authigenic phosphate minerals (Shemesh, 1990). It is thus not surprising that authigenic apatite that formed within marine sediment during the Cambrian is now operationally classified as crystalline igneous and metamorphic apatite (sensu Föllmi et al., 2005). Second, within mud-supported, suspension-deposited carbonate, apatite occurs as coarse-silt– to medium-sand–size grains. Given that we observe no comparable-size detrital siliciclastic grains, we suggest that these grains represent eroded, transported, and winnowed authigenic grains. Third, if the P_{xl} phase consisted of fluorapatite provided to the basin along with a detrital siliciclastic influx, we would predict that it should correlate with the siliciclastic-associated heavy element Zr/Al ratio. We observe no correlation between P_{xl} and Zr/Al (Fig. 5F). Thus, consistent with petrographic observations, we conclude that the P_{xl} pool largely represents authigenic apatite, and, therefore, we must account for this phase with a delivery shuttle of P to the sediment column.

Bioclastic Apatite as a Source of Phosphorus for Authigenic Apatite Precipitation?

Lingulid brachiopods comprise a fraction of the bioclasts identified in samples analyzed petrographically for carbonate sedimentology and apatite distribution. The presence of these phosphatic bioclasts raises two issues. First, samples that contain apatite bioclasts will have a wt% P_T that overestimates the quantity of authigenic apatite. Determining the actual wt% of P within authigenic apatite for these samples would require subtracting the wt% of bioclastic P from the bulk wt% P_T determined by phosphorus-speciation geochemistry. One method for determining the wt% of P within primary phosphatic bioclasts would be to use quantitative point-count data to determine the volume of bioclasts and then multiply this volume by the density of dahllite to determine the mass (wt%) of P. Given that the percent of primary phosphatic bioclasts visually (qualitatively) rarely exceeds the percent of phosphatic steinkerns and sand-sized authigenic grains (see earlier discussion), we move forward without quantitative estimates of the wt% of bioclastic P under the caveat that, for lingulid brachiopod–bearing bioclastic lithologies, P_T overestimates authigenic apatite within a sample.

Second, the observation of bioclasts of primary phosphatic shells raises the possibility that in situ dissolution of these bioclasts may have contributed to high pore-water phosphate concentration and facilitated subsequent authigenic precipitation. However, petrographic observations show that inarticulate brachiopod and other phosphatic skeletons are not unusually abundant in phosphate-rich Thorntonia horizons, and conversely that authigenic phosphate is not unusually abundant in those samples with the highest abundances of phosphatic skeletons, nor do these remains show marked evidence of dissolution. Thus, the sedimentation of phosphatic skeletal material does not seem capable of supplying the phosphate now found in Thorntonia rocks. Further, in situ dissolution of phosphatic bioclasts would necessitate pore fluids that promoted the early dissolution of apatite shells without concurrent dissolution of the calcium carbonate shells and sediment molded and/or replaced by the precipitation of authigenic calcium phosphate minerals. For these reasons, we do not invoke phosphatic skeleton–derived P as a significant source for authigenic apatite precipitation. Nevertheless, if phosphatic skeleton dissolution were to have supplied P for authigenic apatite, then the required quantity of organic and iron-bound P (discussed later herein) would lessen proportionately.

Organic-Bound Phosphorus as a Source of Phosphorus for Authigenic Apatite Precipitation?

Particulate organic carbon represents the main delivery shuttle of phosphorus to the sediment column in the modern ocean (e.g., Delaney, 1998; Benitez-Nelson, 2000), and so we ask whether organic carbon could have supplied the observed amount of P within beds of the Thorntonia Limestone and the Arthur Creek Formation. Perhaps the simplest model for organic-bound P delivery is to assume that organic matter arrived at the seafloor with a Redfield C_{org}:P_{org} molar ratio of ~106:1 (Redfield, 1958). However, the C_{org}:P_{org} ratio of organic matter within marine sediment and, therefore, sedimentary rocks, is commonly much higher than the Redfield ratio as a result of the preferential remineralization of P-rich organic compounds within the water column (Clark et al., 1998) or within the sediment column (Ingall et al., 1993; Ingall and Jahnke, 1997; Van Cappellen and Ingall, 1996; Jilbert et al., 2011). The C_{org}:P_{org} molar ratios within the Thorntonia Limestone range from 79:1 up to 17,000:1 (median [first, third quartile] = 1389:1 [521:1, 3619:1]). Likewise, C_{org}:P_{org} molar ratios within the Arthur Creek Formation range from 43:1 up to 11,770:1 (median [first, third quartile] = 903:1 [360:1, 3372:1]). Thus, C_{org}:P_{org} molar ratios within these lithologies deviate substantially from the Redfield ratio and, at face value, suggest extensive preferential P_{org} loss during organic matter respiration.

When organic respiration occurs within the sediment column, liberated P_{org} may "sink-switch" and precipitate as authigenic phosphate minerals (Ruttenberg and Berner, 1993), as is likely the case for the development of phosphatic strata within the Thorntonia Limestone. With respect to phosphorus-speciation terminology, "sink-switching" would transfer P from the P_{org} phase to either the authigenic P_{xl} or the $P_{auth+carb}$ phase. In that regard, C_{org}:P_T should provide a better estimate of the retention of organic-bound P to the sedimentary environments of the Thorntonia Limestone and Arthur Creek Formation (Ingall et al., 1993; Ruttenberg and Berner, 1993; Anderson et al., 2001; Algeo and Ingall, 2007). The C_{org}:P_T ratio ranges from 0.1 to 16:1 within the Thorntonia Limestone with a median (first, third quartile) value of 2.5:1 (1.2:1, 4.8:1). For the nonphosphatic Arthur Creek Formation, the C_{org}:P_T ratio ranges from 5 to 157:1, with a median (first, third quartile) value of 17.4:1 (7.6:1, 44.5:1). Thus, with the exception of four samples, C_{org}:P_T molar ratios for both the Thorntonia Limestone and the Arthur Creek Formation fall well below the canonical Redfield ratio (Fig. 5D). From this perspective, both the Thorntonia Limestone and the Arthur Creek Formation retain more P than would be expected based on organic matter delivery with a molar C_{org}:P_{org} ratio equal to or greater than the Redfield ratio.

Preferential C_{org} remineralization or hydrocarbon migration relative to P retention may have resulted in a molar C:P_T lower than the Redfield ratio. The required >90% loss of C_{org} (see Eq. 2 below) appears to be common in relatively organic-lean sediment deposited on oxic Cenozoic seafloors (Anderson et al., 2001); however, given the organic carbon content of Thorntonia samples, and accepting sedimentological and geochemical arguments for anoxic deposition of the Thorntonia Limestone (see section titled, "Iron-Bound Phosphorus as a Source of Phosphorus for Authigenic Apatite Precipitation"), such loss would have required massive remine-

alization under anoxic pore-water conditions. The $\delta^{13}C_{carb}$ values do not show the distinctly light values that might be expected in this circumstance (Schrag et al., 2013). Assuming that all phosphorus was delivered via organic matter with a Redfield ratio and was subsequently retained within the sediment column, the discrepancy between the Redfield ratio and the measured $C:P_T$ provides a minimum estimate of C_{org} loss (estimated quantitatively in the section titled "Assessing the Relative Importance of Organic-Bound versus Iron-Bound Phosphorus to Authigenic Apatite Precipitation").

Organic carbon loss may also occur during low-grade metamorphism (Raiswell and Berner, 1987). Since the lithology of the Thorntonia Limestone precludes a confident application of the suggested metrics to account for this loss (Raiswell and Berner, 1987), we cannot evaluate how much this process may have contributed to the discrepancy between measured $C_{org}:P_T$ values and the Redfield ratio. However, we can explore whether an additional phosphorus delivery shuttle augmented organic-bound P delivery to the seafloor during deposition of the Thorntonia Limestone and Arthur Creek Formation. We discuss this possibility in a later section (see section titled, "Assessing the Relative Importance of Organic-Bound versus Iron-Bound Phosphorus to Authigenic Apatite Precipitation").

Notably, phosphatic strata of the middle Thorntonia Limestone have the highest measured wt% TOC and the lightest $\delta^{13}C_{org}$ values preserved within this sedimentary succession (Fig. 4C). A similar relationship has been documented in Proterozoic basins and attributed to differential recycling of organic matter in benthic mats (e.g., Bartley et al., 1998; Guo et al., 2013). Within the Thorntonia Limestone, this relationship may result from a difference in the primary isotopic composition of organic matter supplying phosphatic strata, from variable in situ remineralization of the sedimentary organic carbon reservoir, or from some combination of these two processes. We do not have an independent line of evidence (e.g., compound-specific biomarkers) to distinguish between these possibilities. Instead, we note that acceptance of either of these hypotheses to explain the observed correlation between P content and $\delta^{13}C_{org}$ values makes a prediction for the mechanism of P delivery. For the case of an isotopically distinct organic carbon source to the middle Thorntonia Limestone, the C:P ratio of this source must have been much lower than the canonical Redfield ratio of 106C:1P. For the case of limited C_{org} remineralization within phosphatic strata, an alternative P delivery shuttle to the sediment column must have augmented organic-bound P delivery.

Iron-Bound Phosphorus as a Source of Phosphorus for Authigenic Apatite Precipitation?

If our estimates of organic-bound P delivery fail to account for the phosphate necessary for the observed Thorntonia apatite content, what alternative source could supply this P?

A growing body of literature calls upon P adsorbed to the surface or coprecipitated with metal oxides, particularly iron (oxyhydr)oxide particles, as an important shuttle of phosphorus to the seafloor (Berner, 1973; Shaffer, 1986; Feely et al., 1991, 1998; Poulton and Canfield, 2006). Additionally, under anoxic conditions, Fe(II)-phosphates (e.g., vivianite, strengite) may play a more important role for marine P cycling than previously considered (e.g., März et al., 2008; Dellwig et al., 2010; Jilbert and Slomp, 2013). Thus, the release of adsorbed/coprecipitated Fe-bound P to sediment pore waters has previously been invoked as a necessary and significant source of P for sedimentary apatite nucleation (Krom and Berner, 1981; Schuffert et al., 1994, 1998; Slomp et al., 1996; Shen et al., 2000; März et al., 2008; Jilbert and Slomp, 2013).

Could the Fe-P shuttle have augmented organic-bound P delivery to Thorntonia and Arthur Creek sediments? In the modern, oxygenated ocean, iron mobility is generally limited to particulate fluxes of insoluble Fe^{3+} phases (Martin and Meybeck, 1979; Poulton and Raiswell, 2002). Under these conditions, we might predict Fe-bound P delivery to these environments to be proportional to the (predominantly siliciclastic) particulate Fe(III) flux. In contrast, under anoxic conditions, the reductive dissolution of iron (oxyhydr)oxides by dissimilatory iron reduction or by dissolved sulfide during early diagenesis generates soluble Fe^{2+} that is subsequently redistributed to anoxic slope and basinal environments (Canfield et al., 1996; Severmann et al., 2008, 2010; see review in Lyons and Severmann, 2006). This so-called "intrabasin iron shuttle" provides a mechanism for decoupling iron delivery to the seafloor from siliciclastic sources, and, therefore, we hypothesize that it allows for the delivery of P adsorbed to detrital Fe(III) minerals, Fe(II)-phosphate minerals (e.g., März et al., 2008; Dellwig et al., 2010; Jilbert and Slomp, 2013), and P adsorbed to or coprecipitated with Fe(III) minerals formed from the oxidation of ferrous iron in the water column (cf. Mayer and Jarrell, 2000). In this regard, under either an oxic or an anoxic Cambrian water column, Thorntonia and Arthur Creek sediments could have received substantial Fe-bound P; however, we note that the P contribution from the Fe-bound P shuttle would have been larger if these sediments accumulated under an anoxic water column.

The redox state of the southern Georgina Basin water column during deposition of these middle Cambrian strata can be assessed using data on the speciation and enrichment of sedimentary iron minerals. This geochemical method is most commonly applied to fine-grain siliciclastic lithologies, where the ratios of various mineralogical phases are interpreted to reflect specific and calibrated environmental redox conditions (Canfield et al., 1992; Raiswell and Canfield, 1998; Raiswell et al., 2001; Poulton and Raiswell, 2002). On the basis of empirical evidence, Fe_{HR}/Fe_T above 0.38 within fine-grain siliciclastic lithologies indicates sediment accumulation under an anoxic water column (Raiswell and Canfield, 1998; Raiswell et al., 2001; Poulton and Raiswell, 2002), while Fe_{HR}/Fe_T below a value of ~0.22 is suggestive of oxic conditions (Poulton and Raiswell, 2002; Poulton and Canfield, 2011); additionally, in the case of anoxia, Fe_{py}/Fe_{HR} differentiates ferruginous (<0.7–0.8) from euxinic (>0.8) conditions (Anderson and Raiswell, 2004; Poulton et al., 2004; März et al., 2008; Poulton and Canfield, 2011).

The Arthur Creek Formation includes a siliciclastic facies (the "hot shale") that is ideal for iron-based redox proxies (Poulton and Canfield, 2005). Fe_T within the Arthur Creek "hot shale" ranges up to ~2.7 wt% (Fig. 6A), and almost all measured highly reactive iron resides in reduced iron minerals (Figs. 6B and 6C). Fe_{HR}/Fe_T and Fe_{PY}/Fe_{HR} ratios indicate an anoxic, ferruginous redox environment during deposition of the hot shale (Figs. 6A and 6B). In contrast, strata of the interlaminated siliciclastic shale/siltstone and carbonate calcimudstone facies of the Arthur Creek Formation (directly overlying the hot shale) contain a lower siliciclastic component, and this requires special attention in interpreting a paleoredox environment. We note that each iron-speciation sample integrates 3 cm of stratigraphy; therefore, for this lithofacies, our sample preparation method homogenized multiple laminae of pure siliciclastic shale/siltstone and pure carbonate mudstone. Yet, despite the diluting carbonate component, Fe_{HR} is partitioned within this lithofacies in the same proportionality as the hot shale (Figs. 6B and 6C). In this regard, iron-speciation data for this lithofacies of the Arthur Creek Formation are consistent with the anoxic, ferruginous redox environment inferred for the underlying hot shale.

Strata of the Thorntonia Limestone are composed almost entirely of carbonate, and for this reason we do not to interpret these iron-speciation data within the canonical, siliciclastic-derived redox framework. Instead, we emphasize that the black, organic-rich carbonate strata of the middle-upper Thorntonia Limestone (Fig. 2C), biomarker and organic geochem-

istry of the Thorntonia and Arthur Creek petroleum systems (Boreham and Ambrose, 2005), and trace-element data (supplementary information [see footnote 1]) are qualitatively consistent with iron-speciation metrics for the Arthur Creek Formation hot shale (Fig. 6), indicating an anoxic depositional environment during accumulation of the phosphatic middle-upper Thorntonia Limestone. Thus, we conclude that the Fe-oxide–bound P shuttle likely augmented organic-bound P delivery to the Thorntonia and Arthur Creek sediment column. Further, if one accepts the sedimentological and geochemical evidence for sediment accumulation under an anoxic, ferruginous water column, this then allows for the possibility that Fe(II)-phosphates provided a second, potentially significant source of P to Thorntonia sediments.

Nevertheless, the limited contribution of Fe_{ox} to Fe_{HR} in both the Thorntonia Limestone and Arthur Creek Formation in drill core NTGS 99/1 (Fig. 5C), the low P_{Fe} values (Fig. 5B), and the present decoupling of P within the Thorntonia Limestone from Fe_{HR} phases (Fig. 5G) all suggest that any P delivered to Thorntonia sediments via the Fe-P shuttle must have been subsequently decoupled from iron particles within the sediment column. One way to explain this decoupling is through the reductive dissolution of Fe oxides in anoxic pore waters. This suggestion is consistent with petrological observations that require wholesale remobilization of P before precipitation within shell interiors (Figs. 3A and 3B). Thus, the present distribution of P in the Thorntonia Limestone, spatially decoupled from either iron or organic carbon sources, confounds easy attribution to primary source vectors. In the following section, we integrate C, Fe, and P geochemical data to explore the relative contributions from organic-bound and iron-bound P delivery sources.

Assessing the Relative Importance of Organic-Bound versus Iron-Bound Phosphorus to Authigenic Apatite Precipitation

To begin, we estimate whether organic matter degradation alone could provide sufficient phosphorus for the observed apatite content in the Thorntonia Limestone. We then quantify how much of this estimated organic carbon must have been lost through remineralization to reconcile the observed wt% TOC within these strata. To do so, we use a Redfield stoichiometry (Redfield, 1958) to relate the measured sedimentary weight percent phosphorus to the associated flux of organic carbon necessary for this phosphorus delivery. Redfield stoichiometry varies in space and time due to, for instance, taxonomic variability in biomolecular and cellular composition and nutrient availability regulating biosynthetic allocation (e.g., Geider and LaRoche, 2002). Moreover, water-column heterotrophy increases the C:P ratio of particulate organic carbon delivered to the sediment-water interface (Clark et al., 1998). To be conservative, we assumed no water-column remineralization and adopted the canonical Redfield ratio (106C:1P) in our calculations. We also adopted the combined organic-bound and authigenic phosphorus phases determined from the phosphorus-speciation extraction as an estimate of the original flux of phosphorus delivered to the sediment via organic matter. This calculation provides a conservative estimate because we neglected iron-adsorbed and carbonate-bound P as potential sources for authigenic apatite (these can represent primary sources of phosphorus to the sediment column), and we assumed no diffusive loss of phosphate from pore-water contemporaneous with sedimentary apatite authigenesis.

Following these arguments, our estimate for the weight percent organic carbon delivered to the sediment column ($\hat{C}^{*}_{org}$) that can account for the measured phosphorus content is given by:

$$\hat{C}^{*}_{org} = \left(P_{xl} + P_{org}\right) \times R \times \left(\frac{\alpha_C}{\alpha_P}\right), \quad (1)$$

where R is the adopted Redfield ratio, and α_C and α_P represent the molar weights of carbon and phosphorus, respectively (Slomp et al., 2004). We estimate the percentage of organic carbon remineralization necessary to reconcile the difference between the delivery estimate, $\hat{C}^{*}_{org}$, and the measured wt% total organic carbon (C_{org}) within Thorntonia and Arthur Creek rocks (Slomp et al., 2004) as:

$$\%\ \text{loss of}\ \hat{C}^{*}_{org} = \left(\frac{\hat{C}^{*}_{org} - C_{org}}{\hat{C}^{*}_{org}}\right) \times 100. \quad (2)$$

This value represents an estimate of organic carbon remineralization in the time between delivery to the sediment-water interface and lithification. Applying these equations to samples within the phosphorus-enriched middle and upper Thorntonia yields a median $\hat{C}^{*}_{org}$ of 18.6 wt% and a median loss of 97.8% of this estimated delivery flux (Fig. 7). For comparison, applying these equations to samples from the Arthur Creek indicates a median organic carbon loss estimate of 74.0% from a median organic carbon delivery estimate, $\hat{C}^{*}_{org}$, of only 1.1 wt% (Fig. 7). If, instead, we consider more typical ratios of C_{org}:P_{org} delivered to the sediment column, that is, C:P >> 106:1 (Ingall et al., 1993; Van Cappellen and Ingall, 1996; Clark et al., 1998; Algeo and Ingall, 2007), then the required C_{org} delivery ($\hat{C}^{*}_{org}$) and the estimated % $\hat{C}^{*}_{org}$ loss increase proportionally. Likewise, any diffusive/advective loss of phosphate from the sediment column prior to lithification (Ingall et al., 1993; Slomp et al., 2002, 2004) would increase the requisite $\hat{C}^{*}_{org}$ and, thus, the inferred % $\hat{C}^{*}_{org}$ loss.

If organic carbon represented the sole delivery source of phosphorus to the sediment column, what would have been the oxidant demand for the organic carbon remineralization estimated here? Dissimilatory microbial metabolisms couple the remineralization of sedimentary organic carbon to the reduction of an oxidant (primarily O_2, NO_3^-, SO_4^{2-}, and Fe^{3+}; Konhauser, 2007). Thus, a portion of the estimated organic carbon loss can be accounted for in the early diagenetic minerals pyrite and siderite, which form from microbial dissimilatory sulfate and ferric iron respiration, respectively. In the following calculations, we assume the stoichiometry of Fe-(oxyhydr)oxide reduction, where one mole of organic carbon is remineralized per four moles of siderite produced:

$$CH_2O + 8H^+ + 4Fe(OH)_3 \Rightarrow 4Fe^{2+}_{(aq)} + CO_2 + 11H_2O, \quad (3)$$

and

$$4Fe^{2+}_{(aq)} + 4CO_2 + 4H_2O \Rightarrow 4FeCO_3 + 8H^+, \quad (4)$$

and sulfate reduction, where four moles of organic carbon are remineralized per mole of pyrite produced:

$$4CH_2O + 2SO_4^{2-} \Rightarrow 2H_2S + 4HCO_3^-, \quad (5)$$

and

$$Fe^{2+}_{(aq)} + 2H_2S \Rightarrow FeS_2 + 4H^+. \quad (6)$$

We note that if Fe^{2+} for pyrite formation were also reduced locally, it would require additional C_{org} consumption, akin to Equation 3.

To correct for the presence of siderite within samples, we relate the measured molar quantity of siderite to the Fe^{3+} respiration stoichiometries of Equations 3 and 4 to estimate the necessary weight percent of organic carbon consumed to produce this siderite ($C_{siderite}$):

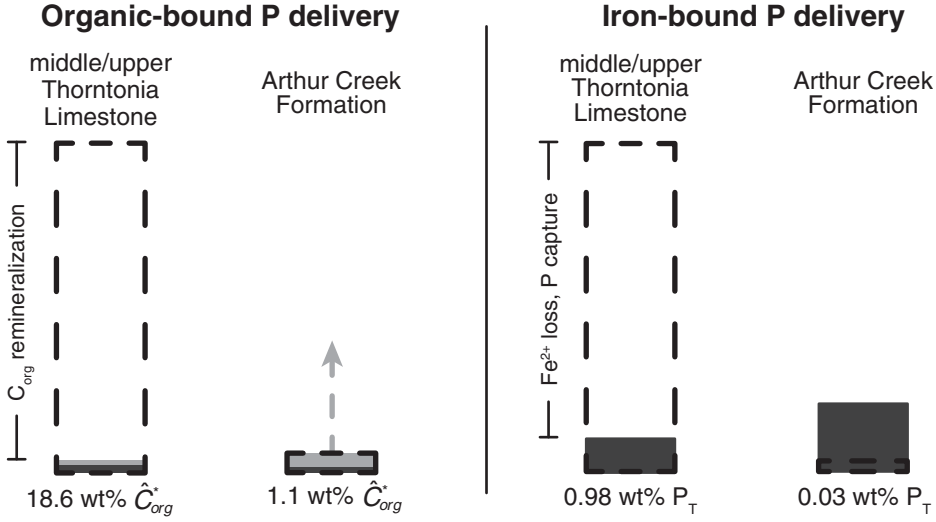

Figure 7. Assessing the potential contribution of organic-bound and iron-bound phosphorus (P) to authigenic apatite precipitation. For the case of organic-bound P delivery (left), the dashed boxes depict the median estimated weight percent organic matter (wt% $\hat{C}^{*}_{org}$) necessary to account for the measured weight percent sedimentary P based on Equation 1 with a Redfield ratio of 106C:1P. Dark-gray boxes represent the median weight percent total organic carbon (TOC) measured within samples. Light-gray boxes represent the corrected weight percent $\hat{C}^{*}_{org}$ (see discussion leading to Equation 9). All values are plotted to scale. Organic carbon delivery can account for all of the P within the Arthur Creek Formation. In contrast, the blank area within the dashed Thorntonia Limestone box represents the amount of $\hat{C}^{*}_{org}$ that would have to have been remineralized to account for the observed sedimentary P content if it were supplied by organic-bound P alone. For the case of iron-bound P delivery (right), the dashed boxes depict the median measured weight percent P_T within samples, while the dark-gray boxes represent the estimated delivery of iron-bound P ($\hat{P}^{*}_{Fe}$) as determined from Equation 13, assuming a partition coefficient for ferrihydrite and a seawater phosphate concentration of 5 μ*M* (see text for discussion). All values are plotted to scale. In this regard, and under these assumptions, the Fe-P delivery shuttle can account for all of the P within the Arthur Creek Formation. In contrast, only by invoking Fe^{2+} loss from the sediment column and preferential capture of Fe-bound P within authigenic phases could the Fe-P shuttle have contributed more substantially (>~10%) to the phosphatic carbonate of the Thorntonia Limestone.

$$C_{siderite} = \left(\frac{\left[\text{measured siderite} \left(\text{mol} \right) \times \left(\frac{1 \text{ mol } C_{org}}{4 \text{ mol siderite}} \right) \right] \times \gamma}{\text{sample weight } \left(g \right)} \right) \times 100, \quad (7)$$

where γ converts measured values in moles to wt%. Likewise, to correct for the presence of pyrite, we relate the measured molar quantity of pyrite within each sample to the stoichiometry of SO_4^{2-} respiration (Eqs. 5 and 6) in order to estimate the weight percent of organic carbon remineralized to produce this pyrite (C_{pyrite}):

$$C_{pyrite} = \left(\frac{\left[\text{measured pyrite } \left(\text{mol} \right) \times \left(\frac{4 \text{ mol } C_{org}}{1 \text{ mol pyrite}} \right) \right] \times \gamma}{\text{sample weight } \left(g \right)} \right) \times 100. \quad (8)$$

Equation 8 does not account for any C_{org} consumed to reduce iron for pyrite (e.g., Eq. 3). In this regard, Equations 8 and 9 conservatively underestimate the weight percent of organic carbon remineralized to form pyrite for the case that iron was reduced locally, rather than supplied as Fe^{2+}.

With these estimates, we augment Equation 2 as:

$$\left(\frac{\hat{C}^{*}_{org} - \left(C_{org} + C_{pyrite} + C_{siderite} \right)}{\hat{C}^{*}_{org}} \right) \times 100. \quad (9)$$

This exercise yields a corrected median % C_{org} loss for the middle and upper Thorntonia members of 96.2%, i.e., not significantly different than the estimate from Equation 2 (Fig. 7). In contrast, and with the exception of phosphorus-enriched samples in the uppermost measured meters, the corrected median loss for the Arthur Creek Formation indicates that there is an excess wt% of organic carbon to account for the observed wt% phosphorus (Fig. 7). However, the observed quantity of siderite within Thorntonia and Arthur Creek samples may represent a late diagenetic addition to the sediment column and, thus, may not have formed through local iron respiration consuming C_{org}. If this were the case, the % C_{org} loss would be less than the value estimated by Equation 9, and closer to the value determined by Equation 2.

With sulfate and ferric iron accounted for, the only quantitatively important remaining oxidant is molecular oxygen (Konhauser, 2007). In this regard, and if the previous assumptions hold, the implication is that the majority of the hypothesized organic carbon loss was through respiration using molecular oxygen. We define a ratio of the estimate of organic matter consumed through anoxic respiration (that is, with Fe^{3+} and SO_4^{2-}: $C_{siderite}$ and C_{pyrite}, respectively) to the estimate of C_{org} loss not accounted for by this estimated anoxic remineralization. We calculate the ratio of anoxic to oxic respiration as:

$$\frac{\text{anoxic}}{\text{oxic}} \text{ respiration} = \frac{C_{pyrite} + C_{siderite}}{\hat{C}^{*}_{org} - \left(C_{org} + C_{pyrite} + C_{siderite} \right)}. \quad (10)$$

In solving Equation 10, we obtain a median (first, third quartile) value of 0.02 (0.1, 0.4) for the middle and upper Thorntonia members. This is to say that a median 2% of the estimated organic carbon delivery required to supply the observed phosphorus content was remineralized through anoxic pathways—98% must have been remineralized with molecular oxygen to explain the absence of this organic carbon from measured samples. If, however, one assumes a diffusive loss of either sulfide or ferrous iron from the sediment column (i.e., the numerator underestimates the organic carbon consumed by anoxic remineralization), the estimated percent of anoxic remineralization becomes a minimum. If such diffusive loss occurred, then the proportion of C_{org} remineralized through oxic respiration would be less than 98% and approach 0% as the sedimentary

production of sulfide and/or Fe^{2+} through microbial dissimilatory redox reactions quantitatively consumed $\hat{C}^{*}_{org}$. While we cannot determine the diffusive flux of reductants from Thorntonia or Arthur Creek sediments based on preserved geochemical signals, we note that such a diffusive loss would be possible if the redox boundary resided within the water column.

The calculated weight percent organic carbon required to deliver the observed phosphorus is notable; the median value, 18.6 wt%, exceeds organic carbon export to the seafloor in most modern marine environments (Hedges and Keil, 1995). While such low organic carbon preservation efficiencies (or, as we describe, high % $\hat{C}^{*}_{org}$ loss estimates) commonly occur within modern marine environments, they typify depositional environments with low sediment accumulation rates (<~0.02 cm/yr) or oxygenated shelf settings (>20 μ*M* bottom-water O_2; Canfield, 1994; Hedges and Keil, 1995). While we cannot provide unequivocal evidence that substantial aerobic carbon respiration did not consume most of the C_{org} originally delivered to the Thorntonia sediment column, we find it difficult to reconcile how such substantial aerobic respiration could have proceeded without concurrently driving the sediment column anoxic, providing a negative feedback on the efficiency of organic carbon respiration. Moreover, we note that the oxidant demand to remineralize this magnitude of organic carbon is difficult to reconcile with Cambrian oxygen levels, perhaps 15%–50% present atmospheric concentrations (Dahl et al., 2010; Bergman et al., 2004; for alternative views, see Berner, 2006; Garrels and Lerman, 1984). Nevertheless, it remains a possibility that episodes of intense aerobic respiration—and efficient capture of released P within authigenic phases—account for Thorntonia Limestone phosphatic carbonate precipitation (although for a discussion of a Miocene phosphogenic episode in which P from aerobic respiration was ruled out, see Föllmi et al., 2005). If, however, one accepts the conclusion that organic burial alone does not provide an adequate source of phosphorus to the sediment column, then an additional source of P must have been present during Thorntonia deposition.

Phosphorus adsorbed onto and/or coprecipitated with metal-oxide particles provides a second potential source of P to the sediment column, the importance of which depends, in part, on the magnitude of the flux of metal oxides to the sediment column (Shaffer, 1986; Feely et al., 1991, 1998; Poulton and Canfield, 2006). Accordingly, we estimate phosphorus delivery under the assumption of an appreciable iron-bound P flux, for simplicity based entirely on P adsorbed to iron (oxyhydr)oxides. This assumption is consistent with the order-of-magnitude calculations presented earlier; nonetheless, we acknowledge that other metal oxides, particularly manganese, play an important role in the cycling of phosphorus (e.g., Dellwig et al., 2010).

Ideally, iron-speciation measurements could provide the basis for a quantitative estimate of Fe-bound P delivered to the sediment column. However, before we can perform such a calculation, we ask whether the Fe_{ox}, Fe_{mag}, Fe_{carb}, and Fe_{py} pools as determined by iron speciation in carbonate-rich strata of the Thorntonia Limestone and Arthur Creek Formation reflect primary depositional reservoirs, or if postdepositional diagenesis could have converted iron into, out of, or between these phases of the highly reactive iron pool? Specifically, if these lithologies experienced closed-system (with respect to mass) diagenetic remobilization of Fe, then it is likely that appreciable amounts of Fe were transferred between highly reactive iron phases (e.g., the formation of Fe_{carb} and Fe_{py} through the reduction of an Fe_{ox} precursor phase). In this regard, the value for Fe_{HR} would still accurately represent the primary iron pool—and could thus be used in calculations of Fe-bound P delivery—however, calculations involving any individual Fe_{HR} phase (e.g., Fe_{ox}, Fe_{carb}) would not provide robust estimates of Fe-bound P. Alternatively, if these lithologies underwent open-system diagenesis, the resulting addition or loss of Fe from the Fe_{HR} pool (from any and/or all constituent phases) would render *any* calculation based on the iron-speciation data suspect. While we cannot eliminate the possibility of Fe addition during open-system diagenesis, we note that Fe-speciation data for the Thorntonia Limestone and Arthur Creek Formation are consistent with other redox proxies (see earlier herein), favoring the view that the highly reactive iron species to these rocks record a substantial depositional flux.

In the following discussion, we provide a methodology to address the potential contribution of the Fe-P shuttle to Thorntonia and Arthur Creek sediments under the assumption of limited or closed-system iron diagenesis. To this end, we employ iron-speciation data from these lithologies for illustrative calculations. These calculations provide a consistency argument given that organic-bound P was likely insufficient to account for the measured P content. Throughout this discussion, we introduce and emphasize the caveats inherent to the use of a diagenetically mobile element in these calculations.

The molar ratio of the coprecipitation of phosphorus onto iron (oxyhydr) oxide particles conforms to a distribution coefficient (K_D) model that scales linearly to the ambient seawater phosphate concentration ($[P_{sw}]$) (Feely et al., 1991, 1998; Konhauser et al., 2007):

$$\left(\frac{P}{Fe}\right)_{molar} = K_D \times \left[P_{sw}\right]. \quad (11)$$

Thus, to estimate the delivery of iron-bound phosphorus, $\hat{P}^{*}_{Fe}$, we multiply an estimate of iron-oxide delivery ($\hat{F}e^{*}_{ox}$) by the adsorption coefficient of phosphorus to iron oxides (K_D) for a given estimate of seawater phosphate concentration ($[P_{sw}]$):

$$\hat{P}^{*}_{Fe} = \gamma \hat{F}e^{*}_{ox} \times K_D \times \left[P_{sw}\right], \quad (12)$$

where γ converts measured values (in wt%) to moles as required in the definition of the adsorption coefficient. Within anoxic pore waters, a fraction of the iron oxides delivered to the sediment column will be reduced by dissimilatory iron reduction and converted to ferrous iron, and these ions will either precipitate as pyrite or iron carbonate, or they will advect/diffuse to the overlying water column. Accordingly, a full accounting of $\hat{F}e^{*}_{ox}$ would include all of these conservation and loss terms. The estimate would become a lower bound on $\hat{P}^{*}_{Fe}$ if we ignored the ferrous iron loss flux, which in any event is unconstrained, and included only the measured iron oxide (Fe_{ox}), pyrite (Fe_{py}), and iron-carbonate phases (Fe_{carb}). We note, however, that at least some of the measured Fe (most obviously the Fe_{carb} phase) may have originated from diagenetic remobilization of iron to these carbonates. (For the lower Thorntonia Limestone, Fe_{carb} comprises a median [first, third quartile] of 76.8% [71.3, 81.8] of the total iron pool; in contrast, for the phosphatic middle-upper Thorntonia Limestone and for the Arthur Creek Formation, Fe_{carb} accounts for only 28.7% [22.3, 33.2] and 20% [15.15, 23.5] of Fe_T, respectively.) In this regard, this calculation may overestimate $\hat{P}^{*}_{Fe}$.

Magnetite may form through the reductive dissolution of mixed ferrous–ferric oxide phases (e.g., Zegeye et al., 2012) and, as such, could be considered in the summation of primary iron-oxide minerals ($\hat{F}e^{*}_{ox}$); however, magnetite may also form during prograde metamorphism, in which case inclusion of this phase would overestimate the primary ferric iron flux to the sediment column. We include Fe_{mag} within our calculation because the authigenic pathway likely exceeds weathering and metamorphic overprints for this depositional environment. (Regardless, within NTGS 99/1, magnetite represents a negligible component of Fe_T; therefore, this assumption does not alter the illustrative estimate for $\hat{P}^{*}_{Fe}$.) Therefore, we rewrite Equation 12 in the approximate form:

$$\hat{P}^{*}_{Fe} = \gamma\left(Fe_{ox} + Fe_{py} + Fe_{carb} + Fe_{mag}\right) \times K_D \times \left[P_{sw}\right]. \quad (13)$$

A host of seawater ions—notably silica, trace metals, and rare earth elements—compete with phosphorus for adsorption sites on the surface of iron-oxide particles (e.g., Berner, 1973; Trocine and Trefry, 1988; Olivarez and Owen, 1989; Trefry and Metz, 1989; Feely et al., 1991, 1998; German et al., 1990; Konhauser et al., 2007). Thus, the choice of K_D depends on the assumption of the seawater composition of Cambrian oceans. As these element concentrations are broadly unknown for the Paleozoic Era, we focus here only on the role of the major seawater constituent dissolved silica in competition for iron-surface anion sites. Following Siever's (1992) inference of cristobalite saturation for early Phanerozoic seawater ($[Si_{SW}]$ = 0.67 m*M*), Konhauser et al. (2007) determined experimentally a K_D = 0.0108 for ferrihydrite at this silica saturation state. Notably, the linear range of the K_D model depends on the phosphorus concentration of ambient seawater. At cristobalite saturation, the linearity of the K_D model saturates above ~5 μ*M* $[P_{sw}]$. This is to say that the coprecipitation and delivery of phosphorus bound to iron oxides remain constant at and above this ambient seawater phosphate concentration.

Hence, we adopt $[P_{sw}]$ = 5 μ*M* to calculate a maximum estimate for $\hat{P}^{*}_{Fe}$ at the adopted $[Si_{SW}]$. We emphasize that the chosen value of 5 μ*M* is a simplistic assumption and that water-column phosphorus concentrations are affected by variable environmental factors that are difficult to generalize, even under well-constrained modern conditions. Nevertheless, this adopted phosphate concentration is consistent with modern anoxic environments, including the Black Sea and Cariaco Basin (Shaffer, 1986; Scranton et al., 2006). For example, in the Black Sea, higher phosphate concentrations in the ferruginous chemocline than in the underlying sulfidic waters result from the dissolution of settling iron oxides and the release of adsorbed phosphate (Brewer and Murray, 1973). Similar processes are suggested to explain the phosphate concentrations (up to 9 μ*M* dissolved P) in the ferruginous Lake Matano (Crowe et al., 2008), where the release of Fe(III)-bound P at the chemocline is balanced by the precipitation of Fe(II)-phosphates below the chemocline.

Applying Equation 13 to samples from the middle and upper Thorntonia members yields a median estimate for iron-bound P of 0.1 wt% as compared to a median estimate of 0.2 wt% for the Arthur Creek (Fig. 7). In this formulation, phosphorus delivery by iron oxides is proportional to the highly reactive iron phases (Fe_{HR}) determined from iron-speciation geochemistry. While Fe_{HR}/Fe_T decreases between the P-enriched middle and upper Thorntonia members and the Arthur Creek Formation, the observed increase in Fe_T within the Arthur Creek compensates such that the molar estimate of $\hat{F}e^{*}_{ox}$, and, thus, $\hat{P}^{*}_{Fe}$, remains roughly constant between the two formations. As such, and if the these assumptions hold, this implies that the relative contribution of the Fe-P shuttle to the observed weight percent sedimentary P was much greater during deposition of the Arthur Creek Formation because of the lower wt% P_T measured throughout this formation. Indeed, the median estimate of $\hat{P}^{*}_{Fe}$ = 0.2 wt% for the Arthur Creek Formation greatly exceeds the median measured P_T (0.03 wt%; Fig. 7). In contrast, the median estimate of $\hat{P}^{*}_{Fe}$ = 0.1 wt% for the middle and upper Thorntonia members provides only ~10% of the median measured P_T (0.98 wt%; Fig. 7), and proportionally less for samples with the highest measured P_T approaching 4 wt%. Likewise, any diffusive loss of P from the sediment column prior to lithification would increase the requisite $\hat{P}^{*}_{Fe}$ and, in the case of the Thorntonia sections, increase the deficiency between the observed P_T and P hypothesized to have been delivered associated with Fe_{ox} ($\hat{P}^{*}_{Fe}$).

The formulation of our equations may significantly overestimate Fe-bound P delivery for two reasons. First, our calculations adopt a K_D value based on an estimate of contemporaneous seawater silica concentrations. Second, our calculations adopt a seawater phosphate concentration that maximizes the potential for P delivery by the iron shuttle. If we presumed a higher seawater silica concentration (that is, decreased K_D), or if, for an assumed $[Si_{SW}]$, we also assumed a lower $[P_{SW}]$, then we would calculate a lower P delivery flux per unit Fe_{ox}. Thus, both of these changes would yield a lower estimate of $\hat{P}^{*}_{Fe}$ for a given iron flux to the sediment column.

Some iron minerals are more effective P delivery shuttles than others. The capacity for iron minerals to scavenge and deliver phosphorus to the seafloor depends on a number of factors, including the surface density of adsorption sites, which in part is related to mineral surface area. In this regard, amorphous to poorly crystalline phases will scavenge more phosphate than highly crystalline phases. (We note, however, that progressive crystallization may result in the subsequent desorption of P from adsorption sites. If this desorption occurs within the sediment column, outside the length-scales of advection/diffusion with the overlying water column, Fe-bound P could provide a significant source of P to the sediment column.) Here, we assumed ferrihydrite as the carrier phase (Konhauser et al., 2007); however, several other iron minerals form during anaerobic Fe^{2+} oxidation (e.g., Kappler and Newman, 2004; Zegeye et al., 2012). For instance, in a detailed study of Fe mineralogy in a ferruginous water column (Lake Matano, Indonesia), Zegeye et al. (2012) found that ferrihydrite was quantitatively transformed to carbonated green rust ("fougerite") during settling through the water column, with more minor formation of magnetite. Unfortunately, no experimental data currently exist for P adsorption to green rust under the chemical conditions likely encountered in Cambrian oceans (e.g., Lake Matano has relatively low [Si]). However, adsorption of oxyanions to green rust tends to be far higher than for ferrihydrite (Randall et al., 2001), and thus such a finding highlights the need to consider multiple and varied carrier phases for the ancient Fe-P shuttle. An iron-carrier phase with an adsorption coefficient (K_D) with respect to P greater than ferrihydrite could have delivered more P to Thorntonia sediments for a given iron flux to the seafloor.

Are there other scenarios in which the delivery of Fe-bound P could have been greater than that inferred from the formulations of Equations 11 through 13? To answer this question, it is necessary to address whether the measured Fe_{HR} is an accurate proxy for the contribution of Fe_{ox} to the sediment column, or whether it could underestimate the original Fe_{ox} flux ($\hat{F}e^{*}_{ox}$), and, thus, $\hat{P}^{*}_{Fe}$, to the sediment column. Next, we explore hypothetical redox scenarios in which Fe-bound P could contribute more substantially to authigenic apatite. Without an independent line of evidence that the constituent phases of the highly reactive iron pool represent the primary fluxes of iron to the sediment column, we choose not to advocate for this possibility for the Thorntonia Limestone. Nevertheless, with regard to the broader question of the mechanism for phosphatic carbonate deposition, we find it informative to evaluate the circumstances in which the Fe-bound delivery shuttle could contribute substantially to phosphogenesis and phosphatic carbonate deposition.

One can envision a spectrum of scenarios for the relative magnitudes of Fe_{ox} delivery to and Fe^{2+} loss from the sediment column. These scenarios fall within three generalized categories: Fe_{ox} delivery (1) greater than, (2) nearly equal to, or (3) less than Fe^{2+} diffusive/advective loss. In the following discussion, we discount scenario 3 because such an imbalance defines an unsustainable Fe cycle. To begin, we consider the scenario that (1) Fe_{ox} delivery exceeds Fe^{2+} loss. This can result from two opposing redox regimes. (1a) If the majority of Fe_{ox} delivered to the sediment column were stabilized within oxygenated pore water, then this would preclude widespread iron reduction. In this instance, only a small amount of P would be liberated from the Fe_{ox} delivery shuttle, and Fe_{ox} would dominate Fe_{HR}. (1b) Alternatively, if sedimentary electron donors (e.g., C_{org}) contributed to pore-water anoxia, some fraction of the delivered Fe_{ox}

would be reduced to Fe^{2+}, and any P bound to these Fe_{ox} particles would be released to pore waters. To maintain the low Fe^{2+} loss fraction defining this scenario, any Fe^{2+} ions produced must be captured quantitatively within authigenic ferrous iron minerals. In this instance, sedimentary Fe would be partitioned amongst Fe_{ox}, Fe_{carb}, and Fe_{py} phases, and the dominance of the latter two minerals would imply that much of the original Fe_{ox} flux was reduced. Notably, with regard to P delivery, either scenario for high Fe_{ox} delivery relative to Fe^{2+} loss predicts that the measurement of sedimentary Fe_{HR} represents a close approximation of the magnitude of P delivery associated with the Fe-P shuttle ($\hat{P}^{*}_{Fe}$). If, for example, the Fe cycle were operating in this manner at the time of deposition of the middle and upper Thorntonia members, then, under the above assumptions, the Fe-shuttle would be constrained to have contributed a median of ~10% P_T (as determined from Eq. 13) and, therefore, could not represent a dominant source of P for the observed enrichment.

If scenarios 1a and 1b cannot provide significant amounts of Fe-bound P to phosphatic lithologies, can scenario 2? Like scenario 1b, scenario 2 necessitates a redox environment that facilitates the reductive dissolution of the majority of Fe_{ox} delivered to the sediment column, regardless of the size of this flux. In contrast, scenario 2 is distinguished from scenario 1 by the condition that the majority of the sedimentary Fe^{2+} produced must escape to the overlying water column, resulting in less capture of Fe^{2+} ions in authigenic minerals. Such diffusive loss requires anoxia within the water mass overlying the sediment column. As above, Fe retained within the sediment can reside in any combination of Fe_{ox}, Fe_{carb}, and/or Fe_{py} phases. Notably, scenario 2 allows for the measured Fe_{HR} value to significantly underestimate iron-oxide delivery to the seafloor ($\hat{F}e^{*}_{ox}$) and, therefore, to underestimate the Fe-P shuttle ($\hat{P}^{*}_{Fe}$). If, for example, the Fe cycle were operating with an extensive benthic flux of Fe^{2+} to the water column during deposition of the middle Thorntonia Limestone, and if a mechanism existed to preferentially retain the delivered P, then the Fe-P shuttle could have provided a significant proportion of the observed P to these phosphatic strata, that is, greater than the ~10% estimated from Equation 13.

In summary, simple models of Fe-bound P delivery estimates ($\hat{P}^{*}_{Fe}$), as determined from Equation 13, indicate that this delivery shuttle could have supplied the measured P content of the Arthur Creek Formation. In contrast, our estimates of Fe-bound P can only account for a median of 10% of the P content for the Thorntonia Limestone. (This estimate assumes that Fe_{HR} in Thorntonia rocks reflects deposition from the water column. To the extent that Thorntonia iron minerals reflect open-system diagenesis, this estimate would be even lower.) Only by invoking a major diffusive loss of iron from the Thorntonia sediment column with subsequent capture of delivered P within authigenic phases—a scenario for which we do not advocate, yet do not find inconsistent with the assumption of limited diagenesis—could Fe-bound P have provided a more substantial contribution to phosphatic carbonates of the Thorntonia Limestone.

CONCLUSIONS

Within drill core NTGS 99/1, phosphorus enrichment is confined to the middle and upper members of the Thorntonia Limestone, and petrographic observations reveal that this enrichment reflects authigenic apatite mineral nucleation primarily associated with the interior of bioclasts and, more rarely, as cement in bioclastic grainstone. Under the canonical model that phosphorus bound within organic matter represents the only significant delivery flux of phosphorus to the sediment column, molar C_{org}:P_T well below the Redfield ratio requires significant C_{org} loss or a second delivery source of phosphorus to Thorntonia sediments.

Interpreted together, sedimentological observations and iron-speciation data suggest that sediment within the southern Georgina Basin accumulated under anoxic, ferruginous conditions. This redox diagnosis is consistent with previous research documenting the propensity for anoxic, ferruginous conditions in subsurface water masses of late Neoproterozoic and Cambrian oceans (Canfield et al., 2008) driven by the relative fluxes of electron donors (organic carbon) and electron acceptors (reactive Fe, sulfate) into a basin (Johnston et al., 2010). If correct, the conclusion of an active iron redox cycle contemporaneous with the deposition of the Thorntonia Limestone and Arthur Creek Formation provides a second mechanism for augmented sedimentary phosphorus delivery—phosphorus adsorbed to particulate iron minerals.

The stoichiometries of delivery estimates and remineralization reactions indicate that the phosphorus content of the Arthur Creek Formation is easily accounted for by any combination of phosphorus associated with organic matter and/or iron-oxide fluxes. However, the observed phosphorus content of the Thorntonia Limestone is difficult to reconcile with reasonable fluxes of either organic-bound or iron-bound phosphorus alone. Thus, we suggest that both sources were necessary to account for Thorntonia Limestone phosphatic carbonate deposition.

The discontinuous nature of phosphorite and phosphatic carbonate through Earth history speaks to discontinuous mechanisms of formation. We hypothesize that redox-mediated phosphorus delivery via the Fe-P shuttle, rather than a discontinuous organic carbon flux, provides the more intermittent mechanism for phosphorus delivery to the sediment column. That said, ferruginous bottom waters appear to have been widespread in Proterozoic oceans, whereas phosphatic carbonates are not. Thus, the episodic nature of phosphate deposition must additionally depend on the fate of phosphate after it enters the sediment column. Where the oxic-anoxic interface lies well within the water column, microbial reduction of ferric iron within the sediments will remobilize P, with a high probability of escape back to the water column. Where phosphate in solution is trapped by skeletons, however, or bound to decay-resistant materials such as chitinous exoskeletons, mineral phosphate may be reprecipitated in sediments. With this in mind, it would appear that delivery mechanisms, postdelivery fate within sediments, and evolution all contributed to the observed geological record of Cambrian phosphate accumulation.

ACKNOWLEDGMENTS

We thank the Northern Territory Geological Survey and Max Heckenberg and Jay Carter of the Alice Springs Core Library for generous access to core material. The Agouron Institute and the National Aeronautics and Space Administration (NASA) Astrobiology Institute (Massachusetts Institute of Technology node) provided financial support. We thank Paul Myrow for discussions of sedimentology, Eric Morrow for assistance with data analysis, and Greg Eischeid for technical support in the Harvard University Laboratory for Geochemical Oceanography. We thank David Fike, an anonymous reviewer, and editor A. Hope Jahren for critical comments that helped to improve this paper.

REFERENCES CITED

Algeo, T.J., and Ingall, E., 2007, Sedimentary C_{org}:P ratios, paleocean ventilation, and Phanerozoic atmospheric pO_2: Palaeogeography, Palaeoclimatology, Palaeoecology, v. 256, p. 130–155, doi:10.1016/j.palaeo.2007.02.029.

Ambrose, G.J., Kruse, P.D., and Putman, P.E., 2001, Geology and hydrocarbon potential of the southern Georgina Basin, Australia: Australian Petroleum Production and Exploration Association Journal, v. 41, p. 139–163.

Anderson, L.D., Delaney, M.L., and Faul, K.L., 2001, Carbon to phosphorus ratios in sediments: Implications for nutrient cycling: Global Biogeochemical Cycles, v. 15, p. 65–79, doi:10.1029/2000GB001270.

Anderson, T.F., and Raiswell, R., 2004, Sources and mechanisms for the enrichment of highly reactive iron in euxinic Black Sea sediments: American Journal of Science, v. 304, p. 203–233, doi:10.2475/ajs.304.3.203.

Babcock, L.E., and Shanchi Peng, 2007, Cambrian chronostratigraphy: Current state and future plans: Palaeogeography, Palaeoclimatology, Palaeoecology, v. 254, p. 62–66, doi:10.1016/j.palaeo.2007.03.011.

Bartley, J.K., Pope, M., Knoll, A.H., Semikhatov, M.A., and Petrov, P.Yu., 1998, A Vendian–Cambrian boundary succession from the northwestern margin of the Siberian Platform: Stratigraphy, palaeontology, chemostratigraphy and correlation: Geological Magazine, v. 135, p. 473–494, doi:10.1017/S0016756898008772.

Baturin, G.N., and Bezrukov, P.L., 1979, Phosphorites on the sea floor and their origin: Marine Geology, v. 31, p. 317–332, doi:10.1016/0025-3227(79)90040-9.

Bengtson, S., and Yue Zhao, 1997, Fossilized metazoan embryos from the earliest Cambrian: Science, v. 277, p. 1645–1648, doi:10.1126/science.277.5332.1645.

Bengtson, S., Conway Morris, S., Cooper, B.J., Jell, P.A., and Runnegar, B.N., 1990, Early Cambrian Fossils from South Australia: Association of Australasian Palaeontologists Memoir 9, 364 p.

Benitez-Nelson, C.R., 2000, The biogeochemical cycling of phosphorus in marine systems: Earth-Science Reviews, v. 51, p. 109–135, doi:10.1016/S0012-8252(00)00018-0.

Bergman, N.M., Lenton, T.M., and Watson, A.J., 2004, COPSE: A new model of biogeochemical cycling over Phanerozoic time: American Journal of Science, v. 304, p. 397–437, doi:10.2475/ajs.304.5.397.

Berner, R.A., 1973, Phosphate removal from sea water by adsorption on volcanogenic ferric oxides: Earth and Planetary Science Letters, v. 18, p. 77–86, doi:10.1016/0012-821X(73)90037-X.

Berner, R.A., 2006, GEOCARBSULF: A combined model for Phanerozoic atmospheric O_2 and CO_2: Geochimica et Cosmochimica Acta, v. 70, p. 5653–5664, doi:10.1016/j.gca.2005.11.032.

Bjerrum, C.J., and Canfield, D.E., 2002, Ocean productivity before about 1.9 Gyr ago limited by phosphorus adsorption onto iron oxides: Nature, v. 417, p. 159–162, doi:10.1038/417159a.

Boreham, C.J., and Ambrose, G.J., 2005, Cambrian petroleum systems in the southern Georgina Basin, Northern Territory, Australia, *in* Central Australian Basins Symposium: Petroleum and Minerals Potential: Alice Springs, NT, Australia.

Brasier, M.D., and Callow, R.H.T., 2007, Changes in the patterns of phosphatic preservation across the Proterozoic-Cambrian transition: Association of Australasian Palaeontologists Memoir 34, p. 377–389.

Brewer, P.G., and Murray, J.W., 1973, Carbon, nitrogen and phosphorus in the Black Sea: Deep-Sea Research, v. 20, p. 803–818.

Butterfield, N.J., 2003, Exceptional fossil preservation and the Cambrian explosion: Integrative and Comparative Biology, v. 43, p. 166–177, doi:10.1093/icb/43.1.166.

Canfield, D.E., 1994, Factors influencing organic carbon preservation in marine sediments: Chemical Geology, v. 114, p. 315–329, doi:10.1016/0009-2541(94)90061-2.

Canfield, D.E., Raiswell, R., Westrich, J.T., Reaves, C.M., and Berner, R.A., 1986, The use of chromium reduction in the analysis of reduced inorganic sulfur in sediments and shales: Chemical Geology, v. 54, p. 149–155, doi:10.1016/0009-2541(86)90078-1.

Canfield, D.E., Raiswell, R., and Bottrell, S., 1992, The reactivity of sedimentary iron minerals towards sulfide: American Journal of Science, v. 292, p. 659–683.

Canfield, D.E., Lyons, T.W., and Raiswell, R., 1996, A model for iron deposition to euxinic Black Sea sediments: American Journal of Science, v. 296, p. 818–834, doi:10.2475/ajs.296.7.818.

Canfield, D.E., Poulton, S.W., Knoll, A.H., Narbonne, G.M., Ross, G., Goldberg, T., and Strauss, H., 2008, Ferruginous conditions dominated later Neoproterozoic deep-water chemistry: Science, v. 321, p. 949–952, doi:10.1126/science.1154499.

Clark, L.L., Ingall, E.D., and Benner, R., 1998, Marine phosphorus is selectively remineralized: Nature, v. 393, p. 426, doi:10.1038/30881.

Cook, P.J., 1992, Phosphogenesis around the Proterozoic-Phanerozoic transition: Journal of the Geological Society of London, v. 149, p. 615–620, doi:10.1144/gsjgs.149.4.0615.

Cook, P.J., and McElhinny, M.W., 1979, A re-evaluation of the spatial and temporal distribution of sedimentary phosphate deposits in the light of plate tectonics: Economic Geology and the Bulletin of the Society of Economic Geologists, v. 74, p. 315–330, doi:10.2113/gsecongeo.74.2.315.

Cook, P.J., and Shergold, J.H., 1984, Phosphorus, phosphorites and skeletal evolution at the Precambrian-Cambrian boundary: Nature, v. 308, p. 231–236, doi:10.1038/308231a0.

Cook, P.J., and Shergold, J.H., 1986, Proterozoic and Cambrian phosphorites—Nature and origin, *in* Cook, P.J., and Shergold, J.H., eds., Phosphate Deposits of the Word: Proterozoic and Cambrian Phosphorites, Volume 1: Cambridge, UK, Cambridge University Press, p. 369–386.

Cook, P.J., Shergold, J.H., Burnett, W.C., and Riggs, S.R., 1990, Phosphorite research: A historical overview, *in* Notholt, A.J.G., and Jarvis, I., eds., Phosphorite Research and Development: Geological Society of London Special Publication 52, p. 1–22, doi:10.1144/GSL.SP.1990.052.01.02.

Cordell, D., Drangert, J.-O., and White, S., 2009, The story of phosphorus: Global food security and food for thought: Global Environmental Change, v. 19, p. 292–305, doi:10.1016/j.gloenvcha.2008.10.009.

Crowe, S.A., O'Neill, A.H., Katsev, S., Hehanussa, P., Haffner, G.D., Sundby, B., Mucci, A., and Fowle, D.A., 2008, The biogeochemistry of tropical lakes: A case study from Lake Matano, Indonesia: Limnology and Oceanography, v. 53, p. 319–331, doi:10.4319/lo.2008.53.1.0319.

Dahl, T.W., Hammarlund, E.U., Anbar, A.D., Bond, D.P.G., Gill, B.C., Gordon, G.W., Knoll, A.H., Nielsen, A.T., Schovsbo, N.H., and Canfield, D.E., 2010, Devonian rise in atmospheric oxygen correlated to the radiations of terrestrial plants and large predatory fish: Proceedings of the National Academy of Sciences of the United States of America, v. 107, p. 17,911–17,915, doi:10.1073/pnas.1011287107.

Delaney, M.L., 1998, Phosphorus accumulation in marine sediments and the oceanic phosphorus cycle: Global Biogeochemical Cycles, v. 12, p. 563–572, doi:10.1029/98GB02263.

Dellwig, O., Leipe, T., März, C., Glockzin, M., Pollehne, F., Schnetger, B., Yakushev, E.V., Böttcher, M.E., and Brumsack, H.-J., 2010, A new particulate Mn-Fe-P-shuttle at the redoxcline of anoxic basins: Geochimica et Cosmochimica Acta, v. 74, p. 7100–7115, doi:10.1016/j.gca.2010.09.017.

Donoghue, P., Kouchinsky, A., Waloszek, D., Bengtson, S., Dong, X.-p., Val'kov, A.K., Cunningham, J.A., and Repetski, J.E., 2006, Fossilized embryos are widespread but the record is temporally and taxonomically biased: Evolution & Development, v. 8, p. 232–238, doi:10.1111/j.1525-142X.2006.00093.x.

Dornbos, S.Q., Botjer, D.J., Chen, J.-Y., Gao, F., Oliveri, P., and Li, C.-W., 2006, Environmental controls on the taphonomy of phosphatized animals and animal embryos from the Neoproterozoic Doushantuo Formation, southwest China: Palaios, v. 21, p. 3–14, doi:10.2110/palo.2004.p04-37.

Dunster, J.N., Kruse, P.D., Duffett, M.L., and Ambrose, G.J., 2007, Geology and Resource Potential of the Southern Georgina Basin: Northern Territory Geological Survey Digital Information Package DIP007, 243 p.

Feely, R.A., Trefry, J.H., Massoth, G.J., and Metz, S., 1991, A comparison of the scavenging of phosphorus and arsenic from seawater by hydrothermal iron oxyhydroxides in the Atlantic and Pacific Oceans: Deep-Sea Research, v. 38, p. 617–623, doi:10.1016/0198-0149(91)90001-V.

Feely, R.A., Trefry, J.H., Lebon, G.T., and German, C.R., 1998, The relationship between P/Fe and V/Fe ratios in hydrothermal precipitates and dissolved phosphate in seawater: Geophysical Research Letters, v. 25, p. 2253–2256, doi:10.1029/98GL01546.

Filippelli, G.M., 2011, Phosphate rock formation and marine phosphorus geochemistry: The deep time perspective: Chemosphere, v. 84, p. 759–766, doi:10.1016/j.chemosphere.2011.02.019.

Filippelli, G.M., and Delaney, M.L., 1992, Similar phosphorus fluxes in ancient phosphorite deposits and a modern phosphogenic environment: Geology, v. 20, p. 709–712, doi:10.1130/0091–7613(1992)020<070.

Föllmi, K.B., 1996, The phosphorus cycle, phosphogenesis and marine phosphate-rich deposits: Earth-Science Reviews, v. 40, p. 55–124, doi:10.1016/0012-8252(95)00049-6.

Föllmi, K.B., Badertscher, C., de Kaenel, E., Stille, P., John, C.M., Adatte, T., and Steinmann, P., 2005, Phosphogenesis and organic-carbon preservation in the Miocene Monterey Formation at Naples Beach, California—The Monterey hypothesis revisited: Geological Society of America Bulletin, v. 117, p. 589–619, doi:10.1130/B25524.1.

Garrels, R.M., and Lerman, A., 1984, Coupling of the sedimentary sulfur and carbon cycles; an improved model: American Journal of Science, v. 284, p. 989–1007, doi:10.2475/ajs.284.9.989.

Geider, R., and La Roche, J., 2002, Redfield revisited: Variability of C:N:P in marine microalgae and its biochemical basis: European Journal of Phycology, v. 37, p. 1–17, doi:10.1017/S0967026201003456.

German, C.R., Klinkhammer, G.P., Edmond, J.M., Mitra, A., and Elderfield, H., 1990, Hydrothermal scavenging of rare earth elements in the ocean: Nature, v. 345, p. 516–518, doi:10.1038/345516a0.

Gomez, F.J., Ogle, N., Astini, R.A., and Kalin, R.M., 2007, Paleoenvironmental and carbon-oxygen isotope record of Middle Cambrian carbonates (La Laja Formation) in the Argentine Precordillera: Journal of Sedimentary Research, v. 77, p. 826–842, doi:10.2110/jsr.2007.079.

Guo, H., Du, Y., Kah, L.C., Huang, J., Hu, C., Huang, H., and Yau, W., 2013, Isotopic composition of organic and inorganic carbon from the Mesoproterozoic Jixian Group, North China: Implications for biological and oceanic evolution: Precambrian Research, v. 224, p. 169–183, doi:10.1016/j.precamres.2012.09.023.

Guo, Q., Strauss, H., Liu, C., Zhao, Y., Yang, X., Peng, J., and Yang, H., 2010, A negative carbon isotope excursion defines the boundary from Cambrian Series 2 to Cambrian Series 3 on the Yangtze Platform, South China: Palaeogeography, Palaeoclimatology, Palaeoecology, v. 285, p. 143–151, doi:10.1016/j.palaeo.2009.11.005.

Hedges, J.I., and Keil, R.G., 1995, Sedimentary organic matter preservation: An assessment and speculative synthesis: Marine Chemistry, v. 49, p. 81–115, doi:10.1016/0304-4203(95)00008-F.

Holland, H.D., 2006, The oxygenation of the atmosphere and oceans: Philosophical Transactions of the Royal Society of London, ser. B, Biological Sciences, v. 361, p. 903–915, doi:10.1098/rstb.2006.1838.

Howard, P.F., 1990, The distribution of phosphatic facies in the Georgina, Wiso and Daly River Basins, Northern Australia, *in* Notholt, A.J.G., and Jarvis, I., eds., Phosphorite Research and Development: Geological Society of London Special Publication 52, p. 261–272, doi:10.1144/GSL.SP.1990.052.01.19.

Ingall, E.D., and Jahnke, R.A., 1997, Influence of water-column anoxia on the elemental fractionation of carbon and phosphorus during sediment diagenesis: Marine Geology, v. 139, p. 219–229, doi:10.1016/S0025-3227(96)00112-0.

Ingall, E.D., Bustin, R.M., and Van Cappellen, P., 1993, Influences of water column anoxia on the burial and preservation of carbon and phosphorus in marine shales: Geochimica et Cosmochimica Acta, v. 57, p. 303–316, doi:10.1016/0016-7037(93)90433-W.

Jilbert, T., and Slomp, C.P., 2013, Iron and manganese shuttles control the formation of authigenic phosphorus minerals in the euxinic basins of the Baltic Sea: Geochimica et Cosmochimica Acta, v. 107, p. 155–169, doi:10.1016/j.gca.2013.01.005.

Jilbert, T., Slomp, C.P., Gustafsson, B.G., and Boer, W., 2011, Beyond the Fe-P-redox connection: Preferential regeneration of phosphorus from organic matter as a key control on Baltic Sea nutrient cycles: Biogeosciences, v. 8, p. 1699–1720, doi:10.5194/bg-8-1699-2011.

Johnston, D.T., Poulton, S.W., Dehler, C., Porter, S., Husson, J., Canfield, D.E., and Knoll, A.H., 2010, An emerging picture of Neoproterozoic ocean chemistry: Insights from the Chuar Group, Grand Canyon, USA: Earth and Planetary Science Letters, v. 290, p. 64–73, doi:10.1016/j.epsl.2009.11.059.

Kappler, A., and Newman, D.K., 2004, Formation of Fe(III)-minerals by Fe(II)-oxidizing photoautotrophic bacteria: Geochimica et Cosmochimica Acta, v. 68, p. 1217–1226, doi:10.1016/j.gca.2003.09.006.

Kazakov, A.V., 1937, The phosphate facies: Origin of phosphorites and geological factors of deposit formation: Proceedings of the Scientific Institute of Fertilizers and Insectofungicides, v. 145, p. 1–106.

Konhauser, K.O., 2007, Introduction to Geomicrobiology: Oxford, UK, Blackwell Science, 425 p.

Konhauser, K.O., Lalonde, S.V., Amskold, L., and Holland, H.D., 2007, Was there really an Archean phosphate crisis?: Science, v. 315, p. 1234, doi:10.1126/science.1136328.

Kouchinsky, A., Bengtson, S., Runnegar, B., Skovsted, C., Steiner, M., and Vendrasco, M., 2012, Chronology of Early Cambrian biomineralization: Geological Magazine, v. 149, p. 221–251, doi:10.1017/S0016756811000720.

Krom, M.D., and Berner, R.A., 1981, The diagenesis of phosphorus in a nearshore marine sediment: Geochimica et Cosmochimica Acta, v. 45, p. 207–216, doi:10.1016/0016-7037(81)90164-2.

Laurie, J.R., 2004a, Early Middle Cambrian trilobites from Pacific Oil & Gas Baldwin 1 well, southern Georgina Basin, Northern Territory: Association of Australasian Palaeontologists Memoir 32, p. 127–204.

Laurie, J.R., 2004b, Early Middle Cambrian trilobite faunas from NTGS Elkedra 3 corehole, southern Georgina Basin, Northern Territory: Association of Australasian Palaeontologists Memoir 30, p. 221–260.

Lindsay, J.F., 2002, Supersequences, superbasins, supercontinents—Evidence from the Neoproterozoic–early Palaeozoic basins of central Australia: Basin Research, v. 14, p. 207–223, doi:10.1046/j.1365-2117.2002.00170.x.

Lindsay, J.F., Kruse, P.D., Green, O.R., Hawkins, E., Brasier, M.D., Cartlidge, J., and Corfield, R.M., 2005, The Neoproterozoic–Cambrian record in Australia: A stable isotope study: Precambrian Research, v. 143, p. 113–133, doi:10.1016/j.precamres.2005.10.002.

Lyons, T.W., and Severmann, S., 2006, A critical look at iron paleoredox proxies: New insights from modern euxinic marine basins: Geochimica et Cosmochimica Acta, v. 70, p. 5698–5722, doi:10.1016/j.gca.2006.08.021.

Martin, J.-M., and Meybeck, M., 1979, Elemental mass-balance of material carried by major world rivers: Marine Chemistry, v. 7, p. 173–206, doi:10.1016/0304-4203(79)90039-2.

März, C., Poulton, S.W., Beckmann, B., Küster, K., Wagner, T., and Kasten, S., 2008, Redox sensitivity of P cycling during marine black shale formation: Dynamics of sulfidic and anoxic, non-sulfidic bottom waters: Geochimica et Cosmochimica Acta, v. 72, p. 3703–3717, doi:10.1016/j.gca.2008.04.025.

Mayer, T.D., and Jarrell, W.M., 2000, Phosphorus sorption during iron(III) oxidation in the presence of dissolved silica: Water Research, v. 34, p. 3949–3956, doi:10.1016/S0043-1354(00)00158-5.

Olivarez, A.M., and Owen, R.M., 1989, REE/Fe variations in hydrothermal sediments: Implications for the REE content of seawater: Geochimica et Cosmochimica Acta, v. 53, p. 757–762, doi:10.1016/0016-7037(89)90019-7.

Papineau, D., 2010, Global biogeochemical changes at both ends of the Proterozoic: Insights from phosphorites: Astrobiology, v. 10, p. 165–181, doi:10.1089/ast.2009.0360.

Peng, Shanchi, and Babcock, L.E., 2011, Continuing progress on chronostratigraphic subdivision of the Cambrian System: Bulletin of Geosciences, v. 86, no. 3, p. 391–396, doi:10.3140/bull.geosci.1273.

Planavsky, N.J., Rouxel, O.J., Bekker, A., Lalonde, S.V., Konhauser, K.O., Reinhard, C.T., and Lyons, T.W., 2010, The evolution of the marine phosphate reservoir: Nature, v. 467, p. 1088–1090, doi:10.1038/nature09485.

Porter, S.M., 2004a, Halkieriids in Middle Cambrian phosphatic limestones from Australia: Journal of Paleontology, v. 78, p. 574–590, doi:10.1666/0022-3360(2004)078<0574:HIMCPL>2.0.CO;2.

Porter, S.M., 2004b, Closing the phosphatization window: Testing for the influence of taphonomic megabias on the pattern of small shelly fossil decline: Palaios, v. 19, p. 178–183, doi:10.1669/0883–1351(2004)019<0178.

Poulton, S.W., and Canfield, D.E., 2005, Development of a sequential extraction procedure for iron: Implications for iron partitioning in continentally derived particulates: Chemical Geology, v. 214, p. 209–221, doi:10.1016/j.chemgeo.2004.09.003.

Poulton, S.W., and Canfield, D.E., 2006, Co-diagenesis of iron and phosphorus in hydrothermal sediments from the southern East Pacific Rise: Implications for the evaluation of paleoseawater phosphate concentrations: Geochimica et Cosmochimica Acta, v. 70, p. 5883–5898, doi:10.1016/j.gca.2006.01.030.

Poulton, S.W., and Canfield, D.E., 2011, Ferruginous conditions: A dominant feature of the ocean through Earth's history: Elements, v. 7, p. 107–112, doi:10.2113/gselements.7.2.107.

Poulton, S.W., and Raiswell, R., 2002, The low-temperature geochemical cycle of iron: From continental fluxes to marine sediment deposition: American Journal of Science, v. 302, p. 774–805, doi:10.2475/ajs.302.9.774.

Poulton, S.W., Fralick, P.W., and Canfield, D.E., 2004, The transition to a sulphidic ocean ~1.84 billion years ago: Nature, v. 431, p. 173–177, doi:10.1038/nature02912.

Raiswell, R., and Berner, R.A., 1987, Organic carbon losses during burial and thermal maturation of normal marine shales: Geology, v. 15, p. 853–856, doi:10.1130/0091-7613(1987)15<853:OCLDBA>2.0.CO;2.

Raiswell, R., and Canfield, D.E., 1998, Sources of iron for pyrite formation in marine sediments: American Journal of Science, v. 298, p. 219–245, doi:10.2475/ajs.298.3.219.

Raiswell, R., Newton, R.J., and Wignall, P.B., 2001, An indicator of water-column anoxia: Resolution of biofacies variations in the Kimmeridge Clay (Upper Jurassic, U.K.): Journal of Sedimentary Research, v. 71, p. 286–294, doi:10.1306/070300710286.

Randall, S.R., Sherman, D.M., and Vala Ragnarsdottir, K., 2001, Sorption of As(V) on green rust (Fe4(II)Fe2(III)(OH)12SO_4•3H_2O) and lepidocrocite (γ-FeOOH): Surface complexes from EXAFS spectroscopy: Geochimica et Cosmochimica Acta, v. 65, p. 1015–1023, doi:10.1016/S0016-7037(00)00593-7.

Redfield, A.C., 1958, The biological control of chemical factors in the environment: American Scientist, v. 64, p. 205–221.

Riggs, S.R., 1986, Proterozoic and Cambrian phosphorites—Specialist studies: Phosphogenesis and its relationship to exploration for Proterozoic and Cambrian phosphorites, *in* Cook, P.J., and Shergold, J.H., eds., Phosphate Deposits of the World: Proterozoic and Cambrian Phosphorites, Volume 1: Cambridge, UK, Cambridge University Press, p. 352–368.

Ruttenberg, K.C., 1992, Development of a sequential extraction method for different forms of phosphorus in marine sediments: Limnology and Oceanography, v. 37, p. 1460–1482, doi:10.4319/lo.1992.37.7.1460.

Ruttenberg, K.C., and Berner, R.A., 1993, Authigenic apatite formation and burial in sediments from non-upwelling, continental margin environments: Geochimica et Cosmochimica Acta, v. 57, p. 991–1007, doi:10.1016/0016-7037(93)90035-U.

Saltzman, M.R., 2005, Phosphorus, nitrogen, and the redox evolution of the Paleozoic oceans: Geology, v. 33, p. 573–576, doi:10.1130/G21535.1.

Schrag, D.P., Higgins, J.A., Macdonald, F.A., and Johnston, D.T., 2013, Authigenic carbonate and the history of the global carbon cycle: Science, v. 339, p. 540–543, doi:10.1126/science.1229578.

Schuffert, J.D., Jahnke, R.A., Kastner, M., Leather, J., Sturz, A., and Wing, M.R., 1994, Rates of formation of modern phosphorite off western Mexico: Geochimica et Cosmochimica Acta, v. 58, p. 5001–5010, doi:10.1016/0016-7037(94)90227-5.

Schuffert, J.D., Kastner, M., and Jahnke, R.A., 1998, Carbon and phosphorus burial associated with modern phosphorite formation: Marine Geology, v. 146, p. 21–31, doi:10.1016/S0025-3227(97)00122-9.

Scranton, M.I., McIntyre, M., Astor, Y., Taylor, G.T., Mueller-Karger, F., and Fanning, K., 2006, Temporal variability in the nutrient chemistry of the Cariaco Basin, *in* Neretin, L.N., ed., Past and Present Water Column Anoxia: Berlin, Springer, p. 139–160.

Severmann, S., Lyons, T.W., Anbar, A., McManus, J., and Gordon, G., 2008, Modern iron isotope perspective on the benthic iron shuttle and the redox evolution of ancient oceans: Geology, v. 36, p. 487–490, doi:10.1130/G24670A.1.

Severmann, S., McManus, J., Berelson, W.M., and Hammond, D.E., 2010, The continental shelf benthic iron flux and its isotopic composition: Geochimica et Cosmochimica Acta, v. 74, p. 3984–4004, doi:10.1016/j.gca.2010.04.022.

Shaffer, G., 1986, Phosphate pumps and shuttles in the Black Sea: Nature, v. 321, p. 515–517, doi:10.1038/321515a0.

Shemesh, A., 1990, Crystallinity and diagenesis of sedimentary apatites: Geochimica et Cosmochimica Acta, v. 54, p. 2433–2438, doi:10.1016/0016-7037(90)90230-I.

Shen, Y., Schidlowski, M., and Chu, X., 2000, Biogeochemical approach to understanding phosphogenic events of the terminal Proterozoic to Cambrian: Palaeogeography, Palaeoclimatology, Palaeoecology, v. 158, p. 99–108, doi:10.1016/S0031-0182(00)00033-X.

Siever, R., 1992, The silica cycle in the Precambrian: Geochimica et Cosmochimica Acta, v. 56, p. 3265–3272, doi:10.1016/0016-7037(92)90303-Z.

Slomp, C.P., Epping, E.H.G., Helder, W., and Van Raaphorst, W., 1996, A key role for iron-bound phosphorus in authigenic apatite formation in North Atlantic continental platform sediments: Journal of Marine Research, v. 54, p. 1179–1205, doi:10.1357/0022240963213745.

Slomp, C.P., Thomson, J., and de Lange, G.J., 2002, Enhanced regeneration of phosphorus during formation of the most recent eastern Mediterranean sapropel (S1): Geochimica et Cosmochimica Acta, v. 66, p. 1171–1184, doi:10.1016/S0016-7037(01)00848-1.

Slomp, C.P., Thomson, J., and De Lange, G.J., 2004, Controls on phosphorus regeneration and burial during formation of eastern Mediterranean sapropels: Marine Geology, v. 203, p. 141–159, doi:10.1016/S0025-3227(03)00335-9.

Southgate, P.N., 1988, A model for the development of phosphatic and calcareous lithofacies in the Middle Cambrian Thorntonia Limestone, northeast Georgina Basin, Australia: Australian Journal of Earth Sciences, v. 35, p. 111–130, doi:10.1080/08120098808729443.

Southgate, P.N., and Shergold, J.H., 1991, Application of sequence stratigraphic concepts to Middle Cambrian phosphogenesis, Georgina Basin, Australia: Journal of Australian Geology and Geophysics, v. 12, p. 119–144.

Strickland, J.D.H., and Parsons, T.R., 1972, A Practical Handbook of Seawater Analysis: Fish Research Board of Canada, 310 p.

Swanson-Hysell, N.L., Rose, C.V., Calmet, C.C., Halverson, G.P., Hurtgen, M.T., and Maloof, A.C., 2010, Cryogenian glaciation and the onset of carbon-isotope decoupling: Science, v. 328, p. 608–611, doi:10.1126/science.1184508.

Trappe, J., 2001, A nomenclature system for granular phosphate rocks according to depositional texture: Sedimentary Geology, v. 145, p. 135–150, doi:10.1016/S0037-0738(01)00103-8.

Trefry, J.H., and Metz, S., 1989, Role of hydrothermal precipitates in the geochemical cycling of vanadium: Nature, v. 342, p. 531–533, doi:10.1038/342531a0.

Trocine, R.P., and Trefry, J.H., 1988, Distribution and chemistry of suspended particles from an active hydrothermal vent site on the Mid-Atlantic Ridge at 26°N: Earth and Planetary Science Letters, v. 88, p. 1–15, doi:10.1016/0012-821X(88)90041-6.

Tyrrell, T., 1999, The relative influences of nitrogen and phosphorus on oceanic primary production: Nature, v. 400, p. 525–531, doi:10.1038/22941.

Van Cappellen, P., and Ingall, E.D., 1996, Redox stabilization of the atmosphere and oceans by phosphorus-limited marine productivity: Science, v. 271, p. 493–496, doi:10.1126/science.271.5248.493.

Vine, J.D., and Tourtelot, E.B., 1970, Geochemistry of black shale deposits; a summary report: Economic Geology and the Bulletin of the Society of Economic Geologists, v. 65, no. 3, p. 253–272, doi:10.2113/gsecongeo.65.3.253.

Walter, M.R., Veevers, J.J., Calver, C.R., and Grey, K., 1995, Neoproterozoic stratigraphy of the Centralia Superbasin, Australia: Precambrian Research, v. 73, p. 173–195, doi: 10.1016/0301-9268(94)00077-5.

Wang, X., Hu, W., Yao, S., Chen, Q., and Xie, X., 2011, Carbon and strontium isotopes and global correlation of Cambrian Series 2–Series 3 carbonate rocks in the Keping area of the northwestern Tarim Basin, NW China: Marine and Petroleum Geology, v. 28, p. 992–1002, doi:10.1016/j.marpetgeo.2011.01.006.

Xiao, S.H. and Knoll, A.H., 1999, Fossil preservation in the Neoproterozoic Doushantuo phosphorite Lagerstatte, South China: Lethaia, v. 32, p. 219–240, doi:10. 1111/j.1502–3931.1999.tb00541.x.

Xiao, S.H., and Knoll, A.H., 2000, Phosphatized animal embryos from the Neoproterozoic Doushantuo formation at Weng'an, Guizhou, South China: Journal of Paleontology v. 74, p. 767–788, doi:10.1666/0022-3360(2000)074,0767:PA EFTN.2.0 .CO;2.

Zegeye, A., Bonneville, S., Benning, L.G., Sturm, A., Fowle, D.A., Jones, C., Canfield, D.E., Ruby, C., MacLean, L.C., Nomosatryo, S., Crowe, S.A., and Poulton, S.W., 2012, Green rust formation controls nutrient availability in a ferruginous water column: Geology, v. 40, p. 599–602, doi:10.1130/G32959.1.

Zhu, M.-Y., Zhang, J.-M., Li, G.-X., and Yang, A.-H., 2004, Evolution of C isotopes in the Cambrian of China: Implications for Cambrian subdivision and trilobite mass extinctions: Geobios, v. 37, p. 287–301, doi:10.1016/j.geobios.2003.06.001.

Science Editor: A. Hope Jahren
Associate Editor: Troy Rasbury

Manuscript Received 6 November 2012
Revised Manuscript Received 13 August 2013
Manuscript Accepted 30 September 2013

Printed in the USA